11-15-2015

Fibronectin signals through integrin α5β1 to regulate cardiovascular development in a cell type-specific manner.

Dongying Chen
Thomas Jefferson University

Xia Wang
Thomas Jefferson University

Dong Liang
Thomas Jefferson University; Nanjing Maternity and Child Health Care Hospital Affiliated with Nanjing Medical University

Julie Gordon
University of Georgia

Ashok Mittal
Thomas Jefferson University; Jacobi Medical Center of Albert Einstein College of Medicine

HHS Public Access

Author manuscript

Dev Biol. Author manuscript; available in PMC 2017 February 16.

Published in final edited form as:

Dev Biol. 2015 November 15; 407(2): 195–210. doi:10.1016/j.ydbio.2015.09.016.

Fibronectin signals through integrin α5β1 to regulate cardiovascular development in a cell type-specific manner

Dongying Chen[a,b,1], **Xia Wang**[a,1], **Dong Liang**[a,2], **Julie Gordon**[c], **Ashok Mittal**[a,3], **Nancy Manley**[c], **Karl Degenhardt**[d], and **Sophie Astrof**[a,b,*]

[a]Sidney Kimmel Medical College of Thomas Jefferson University, Department of Medicine, Center for Translational Medicine, 1020 Locust Street, Philadelphia, PA 19107, USA

[b]Cell and Developmental Biology graduate program, Sidney Kimmel Medical College of Thomas Jefferson University, Philadelphia, PA 19107, USA

[c]Department of Genetics, University of Georgia, Athens, GA 30602, USA

[d]Children's Hospital of Pennsylvania, University of Pennsylvania, Philadelphia, PA 19107, USA

Abstract

Fibronectin (Fn1) is an evolutionarily conserved extracellular matrix glycoprotein essential for embryonic development. Global deletion of Fn1 leads to mid-gestation lethality from cardiovascular defects. However, severe morphogenetic defects that occur early in embryogenesis in these embryos precluded assigning a direct role for Fn1 in cardiovascular development. We noticed that Fn1 is expressed in strikingly non-uniform patterns during mouse embryogenesis, and that its expression is particularly enriched in the pharyngeal region corresponding with the pharyngeal arches 3, 4, and 6. This region bears a special importance for the developing cardiovascular system, and we hypothesized that the localized enrichment of Fn1 in the pharyngeal region may be essential for cardiovascular morphogenesis. To test this hypothesis, we ablated Fn1 using the Isl1^{Cre} knock-in strain of mice. Deletion of Fn1 using the Isl1^{Cre} strain resulted in defective formation of the 4th pharyngeal arch arteries (PAAs), aberrant development of the cardiac outflow tract (OFT), and ventricular septum defects. To determine the cell types responding to Fn1 signaling during cardiovascular development, we deleted a major Fn1 receptor, integrin α5 using the Isl1^{Cre} strain, and observed the same spectrum of abnormalities seen in the Fn1 conditional mutants. Additional conditional mutagenesis studies designed to ablate integrin α5 in distinct cell types within the Isl1^{+} tissues and their derivatives, suggested that the expression of integrin α5 in the pharyngeal arch mesoderm, endothelium, surface ectoderm and the neural crest were not required for PAA formation. Our studies suggest that an (as yet unknown) integrin

*Corresponding author at: Sidney Kimmel Medical College of Thomas Jefferson University, Department of Medicine, Center for Translational Medicine, 1020 Locust Street, Philadelphia, PA 19107, USA. Fax: +1 215 955 1690. sophie.astrof@jefferson.edu (S. Astrof).

[1]Contributed equally to this work.

[2]Current address: State Key Laboratory of Reproductive Medicine, Department of Prenatal Diagnosis, Nanjing Maternity and Child Health Care Hospital Affiliated with Nanjing Medical University, 123 Tianfei Street, Nanjing 210029, China.

[3]Current address: Jacobi Medical Center of Albert Einstein College of Medicine, Department of Medicine, Bronx, NY, USA.

Appendix A. Supplementary material

Supplementary data associated with this article can be found in the online version at http://dx.doi.org/10.1016/j.ydbio.2015.09.016.

α5-dependent signal extrinsic to the pharyngeal endothelium mediates the formation of the 4th PAAs.

Graphical abstract

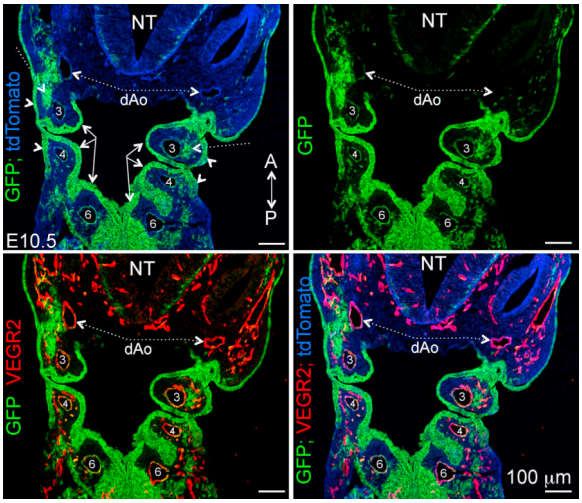

Keywords

Fibronectin; Integrin α5; Cardiovascular development; Pharyngeal arch arteries

1. Introduction

Congenital heart disease (CHD) is a common birth defect, with an incidence of nearly 1% in newborns (Roger et al, 2011). The spectrum of abnormalities observed in CHD includes defects in the morphogenesis of the aortic arch arteries (AAAs). Interruption of the aortic arch is one of the most severe of these defects and is lethal unless corrected by surgery (Moon, 2006, 2008). AAAs are an asymmetrical vascular tree that routes oxygenated blood from the heart to the rest of the body. These blood vessels develop from three pairs of pharyngeal arch arteries (PAAs) – numbered 3, 4, and 6 – that are initially organized symmetrically around the midline (Kirby, 2007). Both the formation of PAAs and their subsequent asymmetrical remodeling are necessary for proper AAA morphogenesis. In this respect, mouse models of CHD indicated that AAA defects in patients with DiGeorge syndrome were likely due to aberrant. PAA formation (Lindsay and Baldini, 2001; Lindsay et al., 2001; Papangeli and Scambler, 2013a), while AAA defects in patients with Allagile syndrome were likely the result of defective PAA remodeling (High and Epstein, 2008). Taken together, these studies indicated that AAA morphogenesis is regulated over multiple steps during embryo development. Therefore, understanding the genes and mechanisms that regulate distinct steps in AAA morphogenesis will provide important insights into the etiology of CHD.

Global Fn1-null embryos arrest their development by E9.5 and die from severe cardiovascular defects (George et al., 1997; George et al., 1993). These embryos exhibit

abnormal left-right patterning, defective development of the definitive endoderm, cardiac outflow tract, and cardiac neural crest (Mittal et al., 2010, 2013; Pulina et al., 2011, 2014; Villegas et al., 2013). However, it remained unclear whether cardiac and vascular defects observed in global Fn1-null embryos resulted directly from the role of Fn1 in cardiovascular development or from the earlier role of Fn1 in embryonic morphogenesis.

Integrins are a major class of Fn1 receptors (Wickstrom et al., 2011; Yang et al., 1999), and at least 10 distinct integrins are known to bind Fn1 (Wickstrom et al., 2011). To understand the mechanisms of Fn1 signal transduction during embryogenesis, several laboratories generated global knockout mice by deleting Fn1 receptors singly or in combination. The phenotypes of integrin α5-null embryos closely resemble those of Fn1-null mutants, while knockouts of other Fn1 receptors (e.g. integrin heterodimers containing αv, α4, α8, or α9 chains) do not correspond with Fn1-null phenotypes (Huang et al., 2009; Wickstrom et al., 2011; Yang et al., 1999). Furthermore, our recent studies indicated that embryonic abnormalities related to defects in the left-right asymmetry, the development of the neural crest, and cardiogenesis in global Fn1-null embryos closely resembled defects observed in integrin α5-nulls (Mittal et al., 2010, 2013; Pulina et al., 2011, 2014; Villegas et al., 2013). Significantly, embryos in which the Arg-Asp-Gly (RGD) integrin-binding site in Fn1 was ablated displayed similar phenotypes when compared with integrin α5-null mutants (Takahashi et al., 2007). These *in vivo* data, along with extensive molecular, biochemical, and cellular studies over the past four decades, have established that integrin α5β1 binds Fn1 and is a major Fn1 signal transducer. However, both the nature of the pathways activated by Fn1-integrin α5β1 interactions *in vivo* and the role(s) of these pathways in cardiovascular morphogenesis are virtually unknown.

In our previous work, we discovered that the expression of Fn1 is dynamically regulated during embryogenesis, and that Fn1 mRNA and protein are distributed in non-uniform patterns within the developing mouse embryo (Mittal et al., 2010; Pulina et al., 2014; Villegas et al., 2013). In particular, we noticed that at E9.5, Fn1 is highly enriched in the pharyngeal arches 3, 4, and 6 (Mittal et al., 2010). Fn1 is essential for vertebrate development and highly evolutionarily conserved (Hynes, 2012; Hynes and Zhao, 2000; Whittaker and Hynes, 2002). Fn1 signals to cells by binding cell-surface integrins and syndecans. Cell adhesion to Fn1 regulates numerous cell biological functions such as proliferation, survival, and migration (Hynes, 2002, 2009; Schwartz, 2010; Schwartz and Assoian, 2001). In addition, Fn1 binds a number of growth factors, including VEGF, HGF, and many Fgfs (Giancotti and Tarone, 2003; Hynes, 2009; Martino and Hubbell, 2010; Miyamoto et al., 1996; Wijelath et al., 2002). Many growth factors require integrin-mediated cell adhesion to Fn1 for signaling (Giancotti and Tarone, 2003; Miyamoto et al., 1996). Taken together, these studies suggest that the enrichment of Fn1 in distinct embryonic regions may be important to modulate cellular responses to growth factors and to regulate specific morphogenetic processes.

To test this hypothesis, we ablated *Fn1* in the pharyngeal region using the Isl1^{Cre} knock-in strain of mice. In this strain, the Cre enzyme mediates recombination in several pharyngeal tissues including the pharyngeal and splanchnic mesoderm, endoderm, surface ectoderm and specific subpopulations of the cardiac neural crest (Cai et al., 2003; Engleka et al., 2012;

Park et al., 2006). Our studies indicate that distinct, cell type-specific pharyngeal sources of Fn1 play a number of distinct, indispensible roles in cardiovascular development and the formation of the 4th pair of PAAs. Moreover, we found that the phenotypes of $Fn1^{flox/-}$; $Isl1^{Cre}$ and integrin $\alpha5^{flox/-}$; $Isl1^{Cre}$ mutants are similar with each other, indicating that integrin $\alpha5\beta1$ acts as a major Fn1 receptor in the pharyngeal tissues. We then employed a series of conditional mutagenesis experiments to identify pharyngeal cell types, in which integrin α5-dependent signals regulate the development of distinct cardiovascular features.

2. Materials and methods

2.1. Mouse strains and genotyping

$Fn1^{+/-}$ mice, integrin $\alpha5^{+/-}$ mice and integrin $\alpha5^{flox/flox}$ mice were a gift from Dr. Richard Hynes (George et al., 1997; van der Flier et al., 2010; Yang et al., 1993). $Fn1^{flox/flox}$ mice were a gift from Dr. Reinhardt Fassler (Sakai et al., 2001). $Isl1^{Cre}$ knock-in mice were a gift from Dr. Sylvia Evans (Cai et al., 2003). $Rosa^{mTmG}$ mice, Gt (ROSA)26Sortm4(ACTB-tdTomato,-EGFP) were purchased from Jackson labs (Muzumdar et al., 2007). $Fn1^{+/-}$ mice or integrin $\alpha5^{+/-}$ mice were crossed with $Isl1^{Cre}$ knock-in mice to generate $Fn1^{+/-}$; $Isl1^{Cre/+}$ or integrin $\alpha5^{+/-}$; $Isl1^{Cre/+}$ males, respectively. To obtain embryos, $Fn1^{flox/flox}$ females were crossed with $Fn1^{+/-}$; $Isl1^{Cre/+}$ males and integrin $\alpha5^{flox/flox}$ females were crossed with integrin $\alpha5^{+/-}$; $Isl1^{Cre/+}$ males. Adult mice and embryos were genotyped as described (Cai et al., 2003; George et al., 1997; Sakai et al., 2001; van der Flier et al., 2010). All experimental procedures were approved by the Institutional Animal Care and Use Committee of Thomas Jefferson University and conducted in accordance with federal guidelines for humane care of animals.

2.2. In situ hybridization

We generated the Fn1 *in situ* hybridization (ISH) probe and performed whole mount ISH staining procedure, as described (Mittal et al., 2010). For the ISH on tissue sections, Fn1 probe recognizing the first exon of the *Fn1* gene was purchased from the Advanced Cell Diagnostics (cat # 316951, ACD, Hayward, CA, USA). Detection was done using RNAscope 2.0 FFPE Assay Brown kit according to the manufacture's protocol. After the signal was developed, sections were counterstained with Gill's hematoxylin.

2.3. Intracardiac injection of India Ink

Embryos were dissected at E10.5 and fixed with 4% paraformaldehyde at 4 °C overnight. Embryos were rinsed with PBS and India ink injections were performed as described (Liang et al., 2014).

2.4. Immunofluorescence staining and histology

Dissected embryos were fixed with 4% paraformaldehyde at 4 °C overnight, rinsed in phosphate buffered saline (PBS), and stored in PBS at 4 °C for no more than 2 weeks. For paraffin embedding, embryos were processed through a graded series of alcohol and xylenes. Hematoxylin and eosin staining as well as alcian blue and nuclear fast red staining were done according to standard protocols. Alternatively, embryos were dehydrated through graded methanol series and stored at − 20 °C. For frozen sections, embryos were incubated

in 30% sucrose in PBS until they sunk and then in 50/50 mix of 30% sucrose and optimum cutting temperature (OCT) compound (Tissue-Tek) at 4 °C overnight. Embryos were embedded in a 50/50 mix of 30% sucrose and OCT and frozen using isopentane/dry ice bath. The following primary antibodies were used to stain frozen sections: anti-integrin α5 (1:200, BD, cat #553319), anti-VEGFR2 (1:200, R&D, cat#AF644), anti-Pecam1 (1:200, BD Pharmingen, cat# 553370), anti-PDGFRβ (1:100; R&D, cat#AF1042), anti-NG2 (1:100, Millipore, cat#05-710), anti-ERG (1:100, Abcam, cat#ab110639). The following antibodies were used for either frozen or paraffin sections: rabbit polyclonal against mouse Fn1 (1:500, a gift from Dr. Richard Hynes lab, MIT) (George et al., 1993), anti-GFP (1:500, Aves labs, cat #GFP-1020). For staining, sections were incubated with blocking buffer consisting of 10% Donkey serum in PBST (0.05% Tween 20 in PBS) for 1 h at room temperature (rt) and then incubated with primary antibodies diluted in blocking buffer overnight at 4 °C. The following day, sections were washed and then incubated with secondary antibodies: anti-mouse, anti-goat, anti-chicken, or anti-rabbit conjugated to Alexa-488, Alexa-555, or Alexa 647 (1:300, Invitrogen), or FITC-conjugated anti-chicken IgY antibodies (Jackson Immunoresearch). Nuclei were either stained with DAPI (1:1000 dilution of 5 mg/ml stock solution in H_2O, Sigma, cat #32670-5MG-F) or DRAQ5 (1:1000 dilution of the stock solution supplied by Cell Signaling Technology, catalog #4048,). To extinguish the native tdTomato and memGFP fluorescence in frozen sections from embryos carrying the $ROSA^{mTmG}$ allele(s), sections were dehydrated through graded series of methanol and cover-slipped using glycerol:methanol (50:50) prior to imaging. For paraffin sections, the native tdTomato and memGFP fluorescence was extinguished by boiling sections in 10 mM Citric acid, pH6, for 10 min prior to staining. Slides were then mounted using ProLong® Gold Antifade (Invitrogen). All fluorescence images were acquired using an Olympus FV500 confocal microscope. Bright field images were acquired using Zeiss Axio Observer inverted microscope and DFC420 digital color camera (Leica).

For whole-mount immunofluorescence, embryos were isolated at E10.5 and fixed in 4% paraformaldehyde at 4 °C overnight. After rinsing, embryos were permeabilized with blocking buffer containing PBS, 0.1% Trixon X-100 (PBS-Triton) and 10% donkey serum at 4 °C overnight. The next day, embryos were incubated with anti-Pecam1 antibody (1:200, BD Pharmingen, cat #550274) for 48 h at 4 °C. Embryos were then washed for 4 to 6 hours using PBS-Triton and then incubated with Alexa-conjugated secondary antibodies (1:300, Invitrogen). Embryos were then washed for 24 h at 4 °C and incubated with DRAQ5 (1:1000) for 48 h. All incubations were performed with gentle rocking. Prior to imaging, embryos were dehydrated using a graded series of methanol and cleared using BABB solution consisting of benzyl alcohol (Sigma B-1042): benzyl benzoate (Sigma B-6630) in a 1:2 ratio. Z-stacks were acquired using an Olympus FV500 confocal microscope and analyzed using Imaris software (Bitplane, USA).

2.5. BrdU labeling

BrdU (Fisher Scientific, cat # BP2508250) was dissolved in PBS at 5 mg/ml. Pregnant females were injected with this solution at the dose of 30 mg of BrdU per 1 kg of mouse body weight when embryos reached E10.5 and were sacrificed 30 min after injection. To

detect BrdU, sections were boiled for 10 min in 10 mM Citric acid solution, pH 6.0, and then stained using rat monoclonal anti-BrdU antibody (1:100, Abcam, cat #ab6326).

2.6. Outflow track measurements

The lengths of the proximal and distal portions of the cardiac outflow tract (OFT) and the height of the left ventricle were measured using the ruler tool in the AxioVision Zeiss image acquisition software as shown in Fig. 10. To account for slight differences in the size of the heart, the OFT measurements were normalized relative to the height of the left ventricle.

2.7. Quantitative RT-PCR

We isolated pharyngeal arches 3–6 from $\alpha5^{flox/+}$; $Isl1^{Cre}$ control and integrin $\alpha5^{flox/-}$; $Isl1^{Cre}$ mutant embryos at E10.5. RNA isolation, RT-PCR, quantification and primers sequences were as reported in (Liang et al., 2014).

2.8. Statistical methods

All statistics were performed using Prism 6 version of Graph-pad software. Data were analyzed using either 2-tailed unpaired Student's *t*-test or 2-tailed Fisher exact test, as indicated in the text and figure legends.

3. Results

3.1. Expression of Fn1 in tissues derived from Isl^+ progenitors is required for cardiovascular morphogenesis

Our previous studies indicated that the expression of *Fn1* mRNA was enriched in the pharyngeal region corresponding with pharyngeal arches 3, 4, and 6 at E9.5 (Mittal et al., 2010). Since the sequence of Fn1 is highly conserved in all vertebrates and is required for cardiovascular morphogenesis, we hypothesized that both tissue-specific synthesis of *Fn1* and signaling by Fn1 to specific tissues were important for embryonic and cardiovascular development.

To test our hypotheses, we conditionally ablated *Fn1* expression using the $Isl1^{Cre}$ knock-in strain. The expression of Cre in this strain mediates loxP-dependent recombination in tissues that closely match those expressing *Fn1* (Fig. 1A–A′, B–B′) and leads to specific ablation of *Fn1* mRNA and protein in the pharyngeal region (Fig. 1B–E, 1B′–E′). The remaining Fn1 protein, as will be discussed later, is synthesized by the neural crest (long arrows in Fig. 1B–E) and in neural crest-derived cells (an open arrowhead in Fig. 1E′). We found that conditional deletion of *Fn1* in $Fn1^{flox/-}$; $Isl1^{Cre}$ mutants resulted in late embryonic/early neonatal lethality in the majority of the cases (Table 1) and displayed a variety of cardiovascular and glandular abnormalities (Fig. 2 and Table 2). Gross dissection of E16.5 mutant and control embryos indicated that the majority of $Fn1^{flox/-}$; $Isl1^{Cre}$ mutants exhibited defects in the morphogenesis of the AAAs, which included the interrupted aortic arch type B (IAA-B) (compare Fig. 2A and F), aberrant origin of the right subclavian artery resulting in retroesophageal right subclavian artery (RERSA) (compare Fig. 2B and G, dotted line underlines RERSA), and defects in the branching of the carotid arteries (compare Fig. 2C and H), Table 2.

In addition to vascular abnormalities, we also found membranous and muscular cardiac ventricular septal defects (VSD) in $n = 6/11$ mutants (compare Fig. 2D–E with Fig. 2I–J). The positions of the great vessels, relative to the left and right ventricles of the heart, were unaffected in the majority of $Fn1^{flox/-}$; $Isl1^{Cre}$ mutants, except in one instance of the double outlet right ventricle (DORV) and one instance of persistent truncus arteriosus (PTA; compare Fig. 2K and M). In addition, most of the mutants developed nodules of subaortic cartilage, $n = 7/11$ (compare Fig. 2K, K′ and 2N, N′), and displayed defects in thymus morphogenesis, $n = 7/11$ (compare Fig. 2L, L′, and 2O, P), Table 2. Myocardial thickness and trabeculation were unaffected in the majority of $Fn1^{flox/-}$; $Isl1^{Cre}$ mutants, $n = 10/11$.

The presence of membranous VSD was previously associated with direct and indirect defects in neural crest development (Hutson and Kirby, 2007). Intriguingly, recent studies using the $Isl1^{Cre}$ knock-in mice showed that Cre recombinase in this strain is activated in some populations of the neural crest-derived cells (Engleka et al., 2012). To test whether Isl1 was expressed in the descendants of neural crest cells invading the cardiac outflow tract (OFT), we performed lineage-tracing studies using $TFAP2\alpha^{IRESCre}$ to label neural crest-derived cells. Simultaneously, we co-labeled sections using the antibodies to Isl1. For these and all other experiments involving immunofluorescence, the native GFP and tdTomato fluorescence due to the expression of the $ROSA^{mTmG}$ reporter was extinguished, as described in Methods. These experiments showed that Isl1 is expressed in the neural crest-derived cells entering the cardiac OFT at E9.5 (Fig. 3A, A′). The majority of the neural crest cells in pharyngeal arches 3 (Fig. 3B, B′) and 4 (Fig. 3C, C′) were Isl1-negative. This was also the case at E10.5 (Fig. 3E–E′). To exclude the mesodermal origin of cells co-expressing TFAP2α and Isl1 in the OFT, we performed lineage tracing using the $Mesp1^{Cre}$ strain (Fig. 3D–D′). Mesp1 is a transcription factor expressed in the earliest known mesodermal progenitors, which give rise to anterior mesodermal derivatives including the myocardium and endocardium of the heart (Saga et al., 2000). These fate-mapping experiments showed that $Isl1^{+}$; GFP^{+} double-positive cells in the OFT, as seen in Fig. 3A–A′, are indeed derived from the neural crest and not from the mesoderm (arrows in Fig. 3D, arrowheads in 3D′). Cells expressing Isl1 in E10.5 pharyngeal arches mainly compose the endoderm, surface ectoderm, arch core mesoderm and PAA endothelium (Fig. 3E–E′ and 3F–F′).

Taken together, these studies suggest that the membranous VSD and the peri-aortic cartilage observed in $Fn1^{flox/-}$; $Isl1^{Cre}$ mutants are a direct consequence of $Isl1^{Cre}$-mediated ablation of *Fn1* in neural crest-derived cells. Indeed, we found that the deletion of Fn1 in the neural crest using either the $TFAP2\alpha^{IRESCre}$ knock-in strain or the P3Pro-Cre transgenic line, resulted in the membranous VSD ($n = 11/32$) and peri-aortic cartilage ($n = 10/12$) (Fig. 4).

Neural crest-derived cells are also known to play a requisite role in thymus development, contributing to the thymic capsule and the pericytes of thymic blood vessels (Foster et al., 2008; Hutson and Kirby, 2007; Le Douarin and Jotereau, 1975). Since $Fn1^{flox/-}$; $Isl1^{Cre}$, $Fn1^{flox/-}$; $TFAP2\alpha^{IRESCre}$ and $Fn1^{flox/-}$; P3Pro-Cre mutants develop thymus defects (Fig. 2L, O, P and Fig. 4C, F, I, L), we examined the lineage relationships of cells composing the thymus. We found that $Isl1^{Cre}$ is activated neither in thymic capsule cells nor in pericytes of thymic blood vessels (Fig. 5A, A′), excluding direct effects on the neural crest-derived cells in the thymi in $Fn1^{flox/-}$; $Isl1^{Cre}$ mutants. Vascularization of thymi in $Fn1^{flox/-}$; $Isl1^{Cre}$

embryos isolated at E16.5 appeared to be similar to that of controls; although, we noticed a somewhat disorganized appearance of pericytes in $n = 2/3$ $Fn1^{flox/-}$; $Isl1^{Cre}$ mutants (compare Fig. 5B, B′ with 5D, D′, and 5C, C′ with 5E, E′). With the bulk of thymic tissue derived from the $Isl1^{+}$ pharyngeal endoderm of the 3rd pouch (Fig. 5A, GFP^{+} cells), our data suggest that thymic defects in $Fn1^{flox/-}$; $Isl1^{Cre}$ mutants are likely due to the direct role of Fn1 in the development of this endodermal tissue and indirect role in the development of neural crest-derived pericytes. Taken together, our data indicate that the expression of *Fn1* in $Isl1^{+}$ cells and their descendants is required for ventricular septation, thymus development, and AAA morphogenesis. These phenotypes fall within a spectrum of abnormalities found in DiGeorge patients (Moon, 2008).

Mouse models of DiGeorge syndrome indicate that AAA defects in DiGeorge patients, including IAA-B and RERSA, result from abnormal formation of the 4th pharyngeal arch arteries (PAAs) (Liao et al., 2004; Lindsay et al., 2001; Merscher et al., 2001; Papangeli and Scambler, 2013a). In order to test whether this was the case in our mutants, we isolated E10.5 embryos at the time when all three pairs of PAAs were well-formed in controls and assayed PAA formation either by performing India ink injections into the hearts or by whole mount immunofluorescence staining and imaging. These assays indicated that the left or the right 4th PAAs were not formed properly in $n = 8/18$ $Fn1^{flox/-}$; $Isl1^{Cre}$ mutants, Table 3 (compare Fig. 6A, B and C, D; compare Fig. 6E, F and Fig. 6G, H; and optical sections in Fig. 6E′, F′ and Fig. 6G′, H′). To determine whether abnormal PAA formation resulted from defective proliferation of endothelial cells, we labeled the embryos with BrdU *in utero* and quantified the proportion of BrdU-positive endothelial cells in the 4th PAAs in controls and $Fn1^{flox/-}$; $Isl1^{Cre}$ mutants. These studies demonstrated that endothelial cell proliferation was similar in mutants and controls (Fig. 6I), indicating that defective formation of the 4th PAA was not due to differences in endothelial cell proliferation. The frequency of the 4th arch PAA defects in $Fn1^{flox/-}$; $Isl1^{Cre}$ mutants (44%) at E10.5 corresponds with the frequency of RERSA and IAA-B observed at E16.5 in $Fn1^{flox/-}$; $Isl1^{Cre}$ embryos (42%, Table 2), indicating that AAA anomalies in these mutants arose from defective formation of the 4th pair of PAAs.

Isl1 protein and the Cre recombinase in the $Isl1^{Cre}$ strain label the pharyngeal endoderm, surface ectoderm, arch core mesoderm and PAA endothelium (Fig. 3E, E′, F, F′; and Supplemental Fig. 1), but not neural crest-derived cells in the pharyngeal arches (Fig. 3 and Sup. Fig. 1). Consistent with these observations, the deletion of *Fn1* in the neural crest did not result in PAA formation defects (Fig. 6J–O′). In these experiments, we used $TFAP2\alpha^{IRESCre}$, in which Cre is active in both the neural crest and the pharyngeal surface ectoderm. Taken together, these experiments indicate that these latter two pharyngeal sources of Fn1 are not required for PAA formation.

3.2. Integrin α5 is a major Fn1 receptor in $Isl1^{+}$ cells and their descendants

$Isl1^{+}$ progenitors contribute to multiple tissues within pharyngeal arches. These tissues comprise the pharyngeal endoderm, mesoderm (including PAA endothelium), and surface ectoderm (compare GFP^{+} patterns in Fig. 7A and B; See Sup. Fig. 1 for the full anterior-posterior view of coronal section through the pharyngeal arches). Fn1 protein expression is

enriched at the tissue borders in the pharyngeal arches (Fig. 7C). Intriguingly, *Fn1* mRNA is particularly highly expressed in the endoderm of the 4th pharyngeal arch (double-headed arrow in Fig. 7D). In order to understand the mechanisms by which pharyngeal Fn1 regulates cardiovascular development, we performed conditional mutagenesis to identify Fn1 receptors and to determine the cell types responding to Fn1 signals in the pharyngeal arches. We focused our attention on integrin α5β1 since we and others have shown that phenotypes of integrin α5-null mice closely resemble those of Fn1-null mutants (George et al., 1993, 1997; Goh et al., 1997; Mittal et al., 2010, 2013; Pulina et al., 2011, 2014; Takahashi et al., 2007; Yang et al., 1999; Yang et al., 1993).

Immunofluorescence staining indicated that integrin α5 is expressed in all pharyngeal cell types (Fig. 7E) and is particularly enriched in the PAA endothelium (e.g. open arrowheads in Fig. 7E and F). To determine whether integrin α5β1 regulated cardiovascular morphogenesis downstream of Fn1, we used the $Isl1^{Cre}$ knock-in mice to ablate integrin α5. This strategy resulted in efficient downregulation of integrin α5 in the surface ectoderm, splanchnic and pharyngeal mesoderm, myocardium, and in the endoderm in integrin $\alpha5^{flox/-}$; $Isl1^{Cre}$ mutants at E8.5 (compare Fig. 8A, A′ and B, B′). At E10.5, we observed downregulation of integrin α5 in the PAA endothelium, endoderm and surface ectoderm in the pharyngeal arches of integrin $\alpha5^{flox/-}$; $Isl1^{Cre}$ mutants (Fig. 8C, D and C′, D′). Taken together, these studies indicate that the use of the $Isl1^{Cre}$ knock-in mice resulted in the downregulation of integrin α5 in the expected cell types.

The deletion of integrin α5 in tissues derived from $Isl1^{+}$ cells was embryonic lethal in the majority of the cases (Table 4), and resulted in phenotypes that closely corresponded with those observed in $Fn1^{flox/-}$; $Isl1^{Cre}$ mutants (Fig. 9), Table 5. Similar to $Fn1^{flox/-}$; $Isl1^{Cre}$ embryos, integrin $\alpha5^{flox/-}$; $Isl1^{Cre}$ mutants displayed defects in AAA morphogenesis (compare Fig. 9A–B and Fig. 9E–F), membranous and muscular VSD (compare Fig. 9C–C′ and Fig. 9G–H), and defects in thymus development (Fig. 9D, I, L). We observed a slightly higher proportion of mutants with abnormal alignment of the great vessels relative to the left and right ventricles in integrin $\alpha5^{flox/-}$; $Isl1^{Cre}$ embryos ($n = 4/10$) than in $Fn1^{flox/-}$; $Isl1^{Cre}$ mutants (compare Fig. 9C, C′ with Fig. 9K, K′, showing double outlet right ventricle in the mutant); see Tables 2 and 5. However, this difference in frequency did not reach statistical significance ($p = 0.14$, 2-tailed Fisher exact test). Membranous VSD ($n = 7/14$), peri-aortic cartilage ($n = 3/12$) and thymus defects ($n = 10/15$) were present in integrin $\alpha5^{flox/-}$; $TFAP2\alpha^{IRESCre}$ mutants (Fig. 9M–R). Peri-aortic cartilage results from the abnormal differentiation of neural crest cells (Gao et al., 2010). Taken together, our data suggest that signaling mediated by Fn1-integrin α5β1 interactions in neural crest cells is important for ventricular septation and suppression of differentiation of neural crest cells into the cartilage.

Analogous to $Fn1^{flox/-}$; $Isl1^{Cre}$ mutants, we found that defective PAA formation at E10.5 was the basis for RERSA and IAA-B defects in integrin $\alpha5^{flox/-}$; $Isl1^{Cre}$ mutants (Fig. 10A–H), Table 6. The left, right, or both PAAs were affected in individual integrin $\alpha5^{flox/-}$; $Isl1^{Cre}$ embryos, Table 6. This is similar to the PAA phenotypes observed with $Fn1^{flox/-}$; $Isl1^{Cre}$ mutants (Fig. 6A–H′). The slight increase in the incidence of bilateral PAA defects in integrin $\alpha5^{flox/-}$; $Isl1^{Cre}$ mutants relative to $Fn1^{flox/-}$; $Isl1^{Cre}$ mutants (Table 6) was not statistically significant ($p = 0.32$, 2-tailed Fisher exact test). As in $Fn1^{flox/-}$; $Isl1^{Cre}$ mutants,

endothelial proliferation was not affected in integrin α5$^{flox/-}$; Isl1^{Cre} embryos (Fig. 10I). Finally, deletion of integrin α5 in the neural crest and surface ectoderm using the TFAP2α^{IRESCre} knock-in strain did not result in PAA formation defects (Fig. 10J–K′). This indicates that signaling by integrin α5 in these tissues is dispensable for PAA formation. Taken together, similarities in the phenotypes between integrin α5$^{flox/-}$; Isl1^{Cre} and Fn1$^{flox/-}$; Isl1^{Cre} mutants suggest that Fn1 regulates cardiac morphogenesis and PAA formation by signaling through integrin α5.

3.3. Integrin α5 does not regulate the expression of Tbx1

Cardiovascular phenotypes of Fn1$^{flox/-}$; Isl1^{Cre} and integrin α5$^{flox/-}$; Isl1^{Cre} mutants fall within the range of phenotypes observed in DiGeorge syndrome. Therefore, we investigated whether integrin α5 regulates the expression of the transcription factor *Tbx1*. The *Tbx1* gene is often deleted or mutated in DiGeorge patients (Moon, 2006, 2008). Heterozygous deletion of *Tbx1* in mice gives rise to defects in the formation of the 4th pair of PAAs and in AAA morphogenesis (Liao et al., 2004; Lindsay and Baldini, 2001; Lindsay et al., 2001; Merscher et al., 2001). However, *Tbx1* expression was unaffected in $n = 4/4$ integrin α5$^{flox/-}$; Isl1^{Cre} mutants, suggesting that *Tbx1* expression is not regulated by integrin α5 signaling in tissues derived from Isl1-expressing cells (Fig. 10L).

3.4. Fn1 and integrin α5 regulate OFT morphogenesis

Proper vascular development is dependent on hemodynamic forces, and hence on the development and function of the heart (Culver and Dickinson, 2010; Lucitti et al., 2007; Luo et al., 2001). Therefore, we examined cardiac development in Fn1$^{flox/-}$; Isl1^{Cre} and integrin α5$^{flox/-}$; Isl1^{Cre} mutants. In our previous studies using global, Fn1-null and integrin α5-null embryos, we discovered that Fn1 and integrin α5 were required for the elongation of the cardiac OFT (Mittal et al., 2013). Since the global ablation of Fn1 or integrin α5 led to multiple embryonic morphogenetic defects, it was not clear whether Fn1 and integrin α5 played direct roles in OFT development. The OFT is derived from Isl1^{+} second heart field cells (Cai et al., 2003). To determine whether defects in PAA formation were correlated with abnormal cardiac morphogenesis, we examined OFT development in E10.5 Fn1$^{flox/-}$; Isl1^{Cre} mutants with defective and normal PAAs. Our data indicate that, on average, the relative lengths of the proximal and distal portions of the OFT were shorter in Fn1$^{flox/-}$; Isl1^{Cre} and integrin α5$^{flox/-}$; Isl1^{Cre} mutants compared with controls (Fig. 11). However, when mutants were examined individually, defective PAAs were present in mutants with normal OFTs and normal PAAs were present in mutants with defective OFT (Fig. 11G). Statistical analysis showed that the presence of short OFT did not correlate with defective PAA formation in the mutants ($p = 0.16$, Fisher exact test). Since myocardial development was unaffected in 91% of our mutants, Tables 2 and 5, we conclude that the roles of Fn1 and integrin α5 in PAA development are independent from their roles in OFT morphogenesis.

3.5. Integrin α5 regulates PAA formation indirectly

In order to identify the cell type(s) in which signaling by integrin α5 regulates PAA formation, we performed a series of conditional mutagenesis studies to ablate integrin α5 in distinct pharyngeal cell types. Since the expression of integrin α5 was downregulated in the PAA endothelium of integrin α5$^{flox/-}$; Isl1^{Cre} mutants (Fig. 8C,C′,D, D′), we tested whether

the expression of integrin α5 in the pharyngeal arch endothelium was required for the formation of the 4th PAA. For these experiments, we used the knock-in Mesp1^{Cre} strain to ablate integrin α5, since Mesp1^{+} progenitors give rise to the entire pharyngeal mesoderm including the PAA endothelium (Liang et al., 2014; Papangeli and Scambler, 2013b). Our published studies indicated that the expression of integrin α5 in Mesp1-derived mesoderm, including the PAA endothelium was not required for PAA formation (Liang et al., 2014). This concurred with the observation that the deletion of integrin α5 in the endothelium using the transgenic Tie2-Cre mice did not cause defects in PAA formation (van der Flier et al., 2010). Taken together, these studies indicate that integrin α5 regulates PAA formation indirectly by signaling from within the cell type(s) other than endothelial cells or the mesoderm. The corollary of these studies is that signaling by Fn1 to the pharyngeal mesoderm and endothelium is not required for PAA formation. Thus, signaling by Fn1 and integrin α5 to other pharyngeal tissues regulates PAA formation indirectly.

We next ablated integrin α5 in the neural crest using the P3-ProCre strain, or simultaneously, in the neural crest and the surface ectoderm using the TFAP2α^{IRESCre} strain. PAA formation was unaffected in these mutants (Fig. 10 and data not shown). Taken together, these data indicate that integrin α5-dependent signaling in a tissue other than the mesoderm, neural crest, and surface ectoderm is important for PAA formation.

Even though, integrin α5 is uniformly expressed by the pharyngeal endoderm (Figs. 7E, inset and 8C, C′), the expression of *Fn1* mRNA is enriched specifically in the endoderm of the 4th pharyngeal arch (Fig. 7D). This expression pattern is consistent with our findings that formation of the 4th PAA is selectively affected in Fn1$^{flox/-}$; Isl1^{Cre} and integrin α5$^{flox/-}$; Isl1^{Cre} mutants, and suggests that integrin α5-dependent signaling by Fn1 to the endoderm of the 4th pharyngeal arch may be particularly important. Although the expression of integrin α5 is lower in the endoderm of the 4th arch compared with other pharyngeal arch cell types (Figs. 7E and 8C′) at E10.5, its levels may be sufficient for signaling, especially, given the presence of enriched levels of *Fn1* mRNA synthesized by these cells (double-headed arrow in Fig. 7D). Thus, we propose a model, wherein an (as yet unknown) integrin α5-dependent signal from the pharyngeal endoderm regulates PAA formation (Fig. 12).

4. Conclusions

Fn1 is highly conserved in all vertebrates (Hynes, 2012; Hynes and Zhao, 2000; Whittaker et al., 2006); it is prominently expressed around embryonic blood vessels, and its vascular expression and alternative splicing are tightly regulated upon injury in adult, reviewed by (Astrof and Hynes, 2009). However, direct roles of Fn1 in the development of the heart and blood vessels were obscured by severe morphogenetic defects that occurred at earlier stages of embryogenesis in global, Fn1-null embryos (George et al., 1997; George et al., 1993; Pulina et al., 2014; Pulina et al., 2011). Our data show that Fn1 regulates the development cardiac and vascular structures, and highlight an intriguing discovery that localized, cell-specific expression of the secreted ECM glycoprotein Fn1 is essential for embryogenesis and cardiovascular development. We found that Fn1 synthesized by Isl1-expressing cells and their descendants is required for the morphogenesis of the cardiac OFT, for the formation of the cardiac interventricular septum, thymus development, and formation of the 4th pair of

PAAs. Integrin α5$^{flox/-}$; Isl1^{Cre} mutants displayed similar defects as Fn1$^{flox/-}$; Isl1^{Cre} embryos, suggesting that integrin α5 acts as a main Fn1 receptor in the pharyngeal region. Taken together, our experiments provide the first evidence for the direct involvement of Fn1 and integrin α5 in the regulation of cardiovascular morphogenesis.

5. Discussion

Pharyngeal arches are composed of cells derived from all three embryonic germ layers and consist of the endoderm, mesoderm, surface ectoderm, and neural crest-derived (Hutson and Kirby, 2007). The PAA endothelium is derived from mesodermal progenitors that express the *Mesp1* transcription factor early in gastrulation (Liang et al., 2014; Papangeli and Scambler, 2013b). While the mechanisms of PAA formation are not well understood, PAA development is known to rely on signaling interactions among all cell types that compose the pharyngeal arch (Astrof, 2013). PAA formation can be regulated directly, by signaling within the mesoderm, and indirectly, by signaling from the pharyngeal epithelia, the endoderm, and the surface ectoderm. For example, PAA formation requires the surface ectoderm to express the *Tbx1* and *Gbx2* transcription factors and the *Fgf8* growth factor (Calmont et al., 2009; Macatee et al., 2003). In the mesoderm, PAA formation requires the expression of *Tbx1, PlexinD1*, as well as activation of Notch and retinoic acid pathways (Gitler et al., 2004; High et al., 2009; Li et al., 2012; Zhang et al., 2009; Zhang et al., 2006). Taken together, these and other studies illustrate the complex intercellular signaling interactions that regulate PAA formation.

In Fn1$^{flox/-}$; Isl1^{Cre} mutants, Fn1 is ablated in the pharyngeal embryonic tissues that include splanchnic and pharyngeal mesoderm, pharyngeal endoderm, surface ectoderm, and select populations of neural crest cells. Which of these source(s) of Fn1 is(are) required for cardiovascular development, and do different sources of Fn1 regulate distinct morphogenetic processes? To address these questions we performed conditional mutagenesis studies by ablating *Fn1* expression in distinct cell types within the expression domain that encompasses Isl1^{+} cells and their descendants. These studies showed that Fn1 expression in neural crest-derived cells, surface ectoderm and their derivatives are important for thymus development, for blocking the differentiation of cardiac neural crest cells into the cartilage, and for the development of the membranous ventricular septum but are not required for the formation of the 4th PAA. Conditional mutagenesis studies to ablate Fn1 in other pharyngeal tissues are currently ongoing.

Identification of cell type(s) that regulate cardiovascular morphogenesis in response to Fn1 is essential for uncovering the downstream pathways engaged by Fn1 *in vivo*. To accomplish this, we first asked whether the expression of integrin α5β1 in Isl1^{+} tissues and their descendants was necessary for cardiovascular development and compared the phenotypes of integrin α5$^{flox/-}$; Isl1^{Cre} embryos with those of Fn1$^{flox/-}$; Isl1^{Cre} mutants. We found that the phenotypes of integrin α5$^{flox/-}$; Isl1^{Cre} embryos are indistinguishable from those of Fn1$^{flox/-}$; Isl1^{Cre} mutants, suggesting that Fn1 expressed by the pharyngeal tissues regulates cardiovascular morphogenesis by signaling through integrin α5β1.

Global mutation in integrin α5 led to severe cardiovascular defects, however, whether integrin α5 played a direct role in cardiovascular development was difficult to discern due to the complicating morphogenetic defects in these embryos (Pulina et al., 2011, 2014; Yang et al., 1993). Conditional knockouts of integrin α5 in a number of different cell types, such as endothelial cells, using the Tie2-Cre transgenic line (van der Flier et al., 2010), in lymphatic endothelial cells and mesodermal precursors of mural cells, using the PDGFRβ-Cre transgenic line (Turner et al., 2014), in the pharyngeal mesoderm and endothelium, using the $Mesp1^{Cre}$ knock-in strain (Liang et al., 2014) and in smooth muscle cells, using the SM22α-Cre transgenic line (Turner et al., 2015), showed that the expression of integrin α5 in these cell types did not affect blood vessel formation. This suggested that concomitant signaling by integrin α5 from multiple cell types may be important for cardiovascular development (van der Flier et al., 2010) and/or that cardiovascular defects in global integrin α5-null embryos arose as a consequence of other embryonic abnormalities in these mutants (Goh et al., 1997; Mittal et al., 2010, 2013; Pulina et al., 2011, 2014; Yang et al., 1993). Consistent with these ideas, the ablation of integrin α5 in multiple cell types using the $Isl1^{Cre}$ knock-in strain demonstrated that integrin α5 expression in multiple pharyngeal tissues plays requisite roles in the regulation of cardiovascular morphogenesis. Particularly interesting is the role of integrin α5 and Fn1 in the formation of the 4th PAA. While we do not yet understand the mechanisms, it is important to note that the roles of integrin α5 and Fn1 in cardiac development are separate from their functions in the formation of the 4th PAAs, since cardiac and PAA defects occurred independently of one another.

To determine the cell types, in which signaling by α5β1 regulates cardiovascular development, we performed conditional mutagenesis studies to ablate integrin α5 in distinct tissues within the Is1-expression domain and its derivatives. We found that the expression of α5β1 in the neural crest or in the Mesp1-derived mesoderm (Liang et al., 2014) was required for the formation of the membranous ventricular septum. These studies suggested that the expression of integrin α5β1 in both the neural crest-derived cells and the mesoderm jointly regulates the development of the membranous ventricular septum. Interestingly, and consistent with the studies of (Haack and Hynes, 2001; Turlo et al., 2012), our work indicates that neither Fn1 nor integrin α5 are required for the migration of NC-derived cells.

Mesp1-derived cells include splanchnic mesoderm and all of the known pharyngeal mesodermal cells and their derivatives, such as the OFT and PAA endothelial cells. Interestingly, the expression of integrin α5 in the Mesp1-derived mesoderm was not required for PAA formation. Similarly, concomitant ablation of integrin α5 in the neural crest-derived cells and the surface ectoderm did not affect the formation of the PAAs. These studies suggest the pharyngeal endoderm as an important integrin α5 expression domain regulating PAA formation.

Fn1 and integrin α5 are prominently expressed in the pharyngeal endoderm at E8.5 (Figs. 1B′, 7D, and 8A–A′). At the later embryonic stages, the expression of integrin α5 diminishes but is clearly detectable in the endoderm of the pharyngeal arches at E10.5 (Figs. 7E and 8C, C′). Remarkably, the expression of *Fn1* mRNA becomes highly enriched in the endoderm of the 4th PAAs at E10.5 (Fig. 7D), potentially explaining why the development of the 4th PAAs is particularly defective in $Fn1^{flox/-}$; $Isl1^{Cre}$ and integrin $\alpha5^{flox/-}$; $Isl1^{Cre}$

mutants. Taken together with our conditional mutagenesis studies, these data suggest that Fn1 synthesized by the endoderm mediates the formation of the 4th PAAs indirectly by signaling to the endoderm of the 4th pharyngeal arch through integrin α5β1. This hypothesis needs to be carefully and directly evaluated in the future, since many factors such as potential differences in strains' genetic backgrounds (all of our mice are on a mixed 129-C57BL/6J background), differences in the efficiency and timing of the genetic deletion, as well as other factors may influence PAA formation in the mutants utilized in our work. As an alternative to our model, concomitant integrin α5-dependent signaling in multiple pharyngeal tissues may be required to mediate PAA formation.

How pharyngeal endoderm may regulate PAA development is currently unknown. However, it is well established that both vasculogenesis and angiogenesis can be regulated by signals extrinsic to endothelial cells (Adams and Alitalo, 2007; Bressan et al., 2009; Garriock et al., 2010; Meadows et al., 2012). By circumventing early embryonic lethality, our conditional mutagenesis strategy will facilitate identification of cellular and molecular mechanisms by which Fn1 and integrin α5β1 regulate embryogenesis and cardiovascular development.

Supplementary Material

Refer to Web version on PubMed Central for supplementary material.

Acknowledgments

We are grateful to Richard Hynes for $Fn1^{+/-}$ and integrin $\beta5^{+/-}$ mice and for providing integrin $\beta5^{flox/flox}$ mice prior to their publication. We thank Reinhardt Fassler for $Fn1^{flox/flox}$ mice, Sylvia Evans $Isl1^{Cre}$ knock-in mice, Jonathan Epstein for P3-ProCre mice, and Anne Moon for TFAP2α^{IRESCre} mice. We thank Shuan-You Hou, Ahab Dababneh, and Sonam Dhiman for help with mouse husbandry. We are grateful to Nathan Astrof for critical reading of the manuscript and Jennifer Wilson from the TJU Writing Center for editorial assistance. We thank Syd Astrof for curiosity and cheerful outlook. This work was supported by the funding from the NIH NHLBI RO1 HL103920, American Heart Association Innovative Research Grant 12IRG9130012, the W. W. Smith Charitable Trust, and the funds from the Weizmann Institute of Science–Thomas Jefferson University Collaboration Program to S.A. X. W. was supported by the American Heart Association Postdoctoral Fellowship 12POST11750033.

References

Adams RH, Alitalo K. Molecular regulation of angiogenesis and lymphangiogenesis. Nat. Rev. Mol. Cell. Biol. 2007; 8:464–478. [PubMed: 17522591]

Astrof, S. Interactions between neural crest-derived cells and extracellular microenvironment during cardiovascular development. In: Desimone, DW., Mecham, RP., editors. Extracellular Matrix in Development. Berlin: Springer Verlag; 2013. p. 105-131.

Astrof S, Hynes RO. Fibronectins in vascular morphogenesis. Angiogenesis. 2009; 12:165–175. [PubMed: 19219555]

Bressan M, Davis P, Timmer J, Herzlinger D, Mikawa T. Notochord-de-rived BMP antagonists inhibit endothelial cell generation and network formation. Dev. Biol. 2009; 326:101–111. [PubMed: 19041859]

Cai CL, Liang X, Shi Y, Chu PH, Pfaff SL, Chen J, Evans S. Isl1 identifies a cardiac progenitor population that proliferates prior to differentiation and contributes a majority of cells to the heart. Dev. Cell. 2003; 5:877–889. [PubMed: 14667410]

Calmont A, Ivins S, Van Bueren KL, Papangeli I, Kyriakopoulou V, Andrews WD, Martin JF, Moon AM, Illingworth EA, Basson MA, Scambler PJ. Tbx1 controls cardiac neural crest cell migration during arch artery development by regulating Gbx2 expression in the pharyngeal ectoderm. Development. 2009; 136:3173–3183. [PubMed: 19700621]

Culver JC, Dickinson ME. The effects of hemodynamic force on embryonic development. Microcirculation. 2010; 17:164–178. [PubMed: 20374481]

Engleka KA, Manderfield LJ, Brust RD, Li L, Cohen A, Dymecki SM, Epstein JA. Islet1 derivatives in the heart are of both neural crest and second heart field origin. Circ. Res. 2012; 110:922–926. [PubMed: 22394517]

Foster K, Sheridan J, Veiga-Fernandes H, Roderick K, Pachnis V, Adams R, Blackburn C, Kioussis D, Coles M. Contribution of neural crest-derived cells in the embryonic and adult thymus. J. Immunol. 2008; 180:3183–3189. [PubMed: 18292542]

Gao Z, Kim GH, Mackinnon AC, Flagg AE, Bassett B, Earley JU, Svensson EC. Ets1 is required for proper migration and differentiation of the cardiac neural crest. Development. 2010; 137:1543–1551. [PubMed: 20356956]

Garriock RJ, Czeisler C, Ishii Y, Navetta AM, Mikawa T. An ante-roposterior wave of vascular inhibitor downregulation signals aortae fusion along the embryonic midline axis. Development. 2010; 137:3697–3706. [PubMed: 20940228]

George EL, Baldwin HS, Hynes RO. Fibronectins are essential for heart and blood vessel morphogenesis but are dispensable for initial specification of precursor cells. Blood. 1997; 90:3073–3081. [PubMed: 9376588]

George EL, Georges-Labouesse EN, Patel-King RS, Rayburn H, Hynes RO. Defects in mesoderm, neural tube and vascular development in mouse embryos lacking fibronectin. Development. 1993; 119:1079–1091. [PubMed: 8306876]

Giancotti FG, Tarone G. Positional control of cell fate through joint integrin/ receptor protein kinase signaling. Annu. Rev. Cell. Dev. Biol. 2003; 19:173–206. [PubMed: 14570568]

Gitler AD, Lu MM, Epstein JA. PlexinD1 and semaphorin signaling are required in endothelial cells for cardiovascular development. Dev. Cell. 2004; 7:107–116. [PubMed: 15239958]

Goh KL, Yang JT, Hynes RO. Mesodermal defects and cranial neural crest apoptosis in alpha5 integrin-null embryos. Development. 1997; 124:4309–4319. [PubMed: 9334279]

Haack H, Hynes RO. Integrin receptors are required for cell survival and proliferation during development of the peripheral glial lineage. Dev. Biol. 2001; 233:38–55. [PubMed: 11319856]

High FA, Epstein JA. The multifaceted role of Notch in cardiac development and disease. Nat. Rev. Genet. 2008; 9:49–61. [PubMed: 18071321]

High FA, Jain R, Stoller JZ, Antonucci NB, Lu MM, Loomes KM, Kaestner KH, Pear WS, Epstein JA. Murine Jagged1/Notch signaling in the second heart field orchestrates Fgf8 expression and tissue-tissue interactions during outflow tract development. J. Clin. Invest. 2009; 119:1986–1996. [PubMed: 19509466]

Huang DW, Sherman BT, Lempicki RA. Systematic and integrative analysis of large gene lists using DAVID bioinformatics resources. Nat. Protoc. 2009; 4:44–57. [PubMed: 19131956]

Hutson MR, Kirby ML. Model systems for the study of heart development and disease. Cardiac neural crest and conotruncal malformations. Semin. Cell Dev. Biol. 2007; 18:101–110. [PubMed: 17224285]

Hynes RO. Integrins: bidirectional, allosteric signaling machines. Cell. 2002; 110:673–687. [PubMed: 12297042]

Hynes RO. The extracellular matrix: not just pretty fibrils. Science. 2009; 326:1216–1219. [PubMed: 19965464]

Hynes RO. Evolution: The evolution of metazoan extracellular matrix. J. Cell Biol. 2012; 196:671–679. [PubMed: 22431747]

Hynes RO, Zhao Q. The evolution of cell adhesion. J. Cell Biol. 2000; 150:F89–F96. [PubMed: 10908592]

Kirby, ML. Cardiac Development. New York: Oxford University Press; 2007.

Le Douarin NM, Jotereau FV. Tracing of cells of the avian thymus through embryonic life in interspecific chimeras. J. Exp. Med. 1975; 142:17–40. [PubMed: 239088]

Li P, Pashmforoush M, Sucov HM. Mesodermal retinoic acid signaling regulates endothelial cell coalescence in caudal pharyngeal arch artery vascu-logenesis. Dev. Biol. 2012; 361:116–124. [PubMed: 22040871]

Liang D, Wang X, Mittal A, Dhiman S, Hou SY, Degenhardt K, Astrof S. Mesodermal expression of integrin alpha5beta1 regulates neural crest development and cardiovascular morphogenesis. Dev. Biol. 2014; 395:232–244. [PubMed: 25242040]

Liao J, Kochilas L, Nowotschin S, Arnold JS, Aggarwal VS, Epstein JA, Brown MC, Adams J, Morrow BE. Full spectrum of malformations in velo-cardio-facial syndrome/DiGeorge syndrome mouse models by altering Tbx1 dosage. Hum. Mol. Genet. 2004; 13:1577–1585. [PubMed: 15190012]

Lindsay EA, Baldini A. Recovery from arterial growth delay reduces penetrance of cardiovascular defects in mice deleted for the DiGeorge syndrome region. Hum. Mol. Genet. 2001; 10:997–1002. [PubMed: 11309372]

Lindsay EA, Vitelli F, Su H, Morishima M, Huynh T, Pramparo T, Jurecic V, Ogunrinu G, Sutherland HF, Scambler PJ, Bradley A, Baldini A. Tbx1 haploinsufficieny in the DiGeorge syndrome region causes aortic arch defects in mice. Nature. 2001; 410:97–101. [PubMed: 11242049]

Lucitti JL, Jones EA, Huang C, Chen J, Fraser SE, Dickinson ME. Vascular remodeling of the mouse yolk sac requires hemodynamic force. Development. 2007; 134:3317–3326. [PubMed: 17720695]

Luo Y, Ferreira-Cornwell M, Baldwin H, Kostetskii I, Lenox J, Lieberman M, Radice G. Rescuing the N-cadherin knockout by cardiac-specific expression of N- or E-cadherin. Development. 2001; 128:459–469. [PubMed: 11171330]

Macatee TL, Hammond BP, Arenkiel BR, Francis L, Frank DU, Moon AM. Ablation of specific expression domains reveals discrete functions of ectoderm- and endoderm-derived FGF8 during cardiovascular and pharyngeal development. Development. 2003; 130:6361–6374. [PubMed: 14623825]

Martino MM, Hubbell JA. The 12th-14th type III repeats of fibronectin function as a highly promiscuous growth factor-binding domain. FASEB J. 2010; 24:4711–4721. [PubMed: 20671107]

Meadows SM, Fletcher PJ, Moran C, Xu K, Neufeld G, Chauvet S, Mann F, Krieg PA, Cleaver O. Integration of repulsive guidance cues generates avascular zones that shape mammalian blood vessels. Circ. Res. 2012; 110:34–46. [PubMed: 22076636]

Merscher S, Funke B, Epstein JA, Heyer J, Puech A, Lu MM, Xavier RJ, De-may MB, Russell RG, Factor S, Tokooya K, Jore BS, Lopez M, Pandita RK, Lia M, Carrion D, Xu H, Schorle H, Kobler JB, Scambler P, Wynshaw-Boris A, Skoultchi AI, Morrow BE, Kucherlapati R. TBX1 is responsible for cardiovascular defects in velo-cardio-facial/DiGeorge syndrome. Cell. 2001; 104:619–629. [PubMed: 11239417]

Mittal A, Pulina M, Hou S, Astrof S. Fibronectin and integrin alpha 5 play requisite roles in cardiac morphogenesis. Dev. Biol. 2013; 381:73–82. [PubMed: 23791818]

Mittal A, Pulina M, Hou SY, Astrof S. Fibronectin and integrin alpha 5 play essential roles in the development of the cardiac neural crest. Mech. Dev. 2010; 127:472–484. [PubMed: 20807571]

Miyamoto S, Teramoto H, Gutkind JS, Yamada KM. Integrins can collaborate with growth factors for phosphorylation of receptor tyrosine kinases and MAP kinase activation: roles of integrin aggregation and occupancy of receptors. J. Cell Biol. 1996; 135:1633–1642. [PubMed: 8978828]

Moon A. Mouse models of congenital cardiovascular disease. Curr. Top. Dev. Biol. 2008; 84:171–248. [PubMed: 19186245]

Moon AM. Mouse models for investigating the developmental basis of human birth defects. Pediatr. Res. 2006; 59:749–755. [PubMed: 16641221]

Muzumdar MD, Tasic B, Miyamichi K, Li L, Luo L. A global double-fluorescent Cre reporter mouse. Genesis. 2007; 45:593–605. [PubMed: 17868096]

Papangeli I, Scambler P. The 22q11 deletion: DiGeorge and velocardiofacial syndromes and the role of TBX1. Wiley Interdiscip. Rev. Dev. Biol. 2013a; 2:393–403. [PubMed: 23799583]

Papangeli I, Scambler PJ. Tbx1 genetically interacts with the transforming growth factor-beta/bone morphogenetic protein inhibitor Smad7 during great vessel remodeling. Circ. Res. 2013b; 112:90–102. [PubMed: 23011393]

Park EJ, Ogden LA, Talbot A, Evans S, Cai CL, Black BL, Frank DU, Moon AM. Required, tissue-specific roles for Fgf8 in outflow tract formation and remodeling. Development. 2006; 133:2419–2433. [PubMed: 16720879]

Pulina M, Liang D, Astrof S. Shape and position of the node and notochord along the bilateral plane of symmetry are regulated by cell-extracellular matrix interactions. Biol. Open. 2014; 3:583–590. [PubMed: 24928429]

Pulina MV, Hou SY, Mittal A, Julich D, Whittaker CA, Holley SA, Hynes RO, Astrof S. Essential roles of fibronectin in the development of the left- right embryonic body plan. Dev. Biol. 2011; 354:208–220. [PubMed: 21466802]

Roger VL, Go AS, Lloyd-Jones DM, Adams RJ, Berry JD, Brown TM, Carne-thon MR, Dai S, de Simone G, Ford ES, Fox CS, Fullerton HJ, Gillespie C, Greenlund KJ, Hailpern SM, Heit JA, Ho PM, Howard VJ, Kissela BM, Kittner SJ, Lackland DT, Lichtman JH, Lisabeth LD, Makuc DM, Marcus GM, Marelli A, Matchar DB, McDermott MM, Meigs JB, Moy CS, Mo-zaffarian D, Mussolino ME, Nichol G, Paynter NP, Rosamond WD, Sorlie PD, Stafford RS, Turan TN, Turner MB, Wong ND, Wylie-Rosett J. Heart disease and stroke statistics—2011 update: a report from the American Heart Association. Circulation. 2011; 123:e18–e209. [PubMed: 21160056]

Saga Y, Kitajima S, Miyagawa-Tomita S. Mesp1 expression is the earliest sign of cardiovascular development. Trends Cardiovasc. Med. 2000; 10:345–352. [PubMed: 11369261]

Sakai T, Johnson KJ, Murozono M, Sakai K, Magnuson MA, Wieloch T, Cronberg T, Isshiki A, Erickson HP, Fassler R. Plasma fibronectin supports neuronal survival and reduces brain injury following transient focal cerebral ischemia but is not essential for skin-wound healing and hemostasis. Nat. Med. 2001; 7:324–330. [PubMed: 11231631]

Schwartz MA. Integrins and extracellular matrix in mechanotransduction. Cold Spring Harb. Perspect. Biol. 2010; 2:a005066. [PubMed: 21084386]

Schwartz MA, Assoian RK. Integrins and cell proliferation: regulation of cyclin-dependent kinases via cytoplasmic signaling pathways. J. Cell Sci. 2001; 114:2553–2560. [PubMed: 11683383]

Takahashi S, Leiss M, Moser M, Ohashi T, Kitao T, Heckmann D, Pfeifer A, Kessler H, Takagi J, Erickson HP, Fassler R. The RGD motif in fibronectin is essential for development but dispensable for fibril assembly. J. Cell Biol. 2007; 178:167–178. [PubMed: 17591922]

Turlo KA, Noel OD, Vora R, Larussa M, Fassler R, Hall-Glenn F, Iruela-Arispe ML. An essential requirement for beta1 integrin in the assembly of extracellular matrix proteins within the vascular wall. Dev. Biol. 2012; 365:23–35. [PubMed: 22331032]

Turner CJ, Badu-Nkansah K, Crowley D, van der Flier A, Hynes RO. In-tegrin-alpha5beta1 is not required for mural cell functions during development of blood vessels but is required for lymphatic-blood vessel separation and lymphovenous valve formation. Dev. Biol. 2014; 392:381–392. [PubMed: 24858485]

Turner CJ, Badu-Nkansah K, Crowley D, van der Flier A, Hynes RO. al-pha5 and alphav integrins cooperate to regulate vascular smooth muscle and neural crest functions in vivo. Development. 2015; 142:797–808. [PubMed: 25670798]

van der Flier A, Badu-Nkansah K, Whittaker CA, Crowley D, Bronson RT, Lacy-Hulbert A, Hynes RO. Endothelial alpha5 and alphav integrins cooperate in remodeling of the vasculature during development. Development. 2010; 137:2439–2449. [PubMed: 20570943]

Villegas SN, Barrios-Llerena ME, Pulina M, Hadjantonakis AK, Le Bihan T, Astrof S, Brickman JM. PI3K/Akt1 signalling specifies foregut precursors by generating regionalized extra-cellular matrix. eLife. 2013; 2:e00806. [PubMed: 24368729]

Whittaker CA, Bergeron KF, Whittle J, Brandhorst BP, Burke RD, Hynes RO. The echinoderm adhesome. Dev. Biol. 2006; 300:252–266. [PubMed: 16950242]

Whittaker CA, Hynes RO. Distribution and evolution of von Willebrand/ integrin A domains: widely dispersed domains with roles in cell adhesion and elsewhere. Mol. Biol. Cell. 2002; 13:3369–3387. [PubMed: 12388743]

Wickstrom SA, Radovanac K, Fassler R. Genetic analyses of integrin signaling. Cold Spring Harb. Perspect. Biol. 2011; 3

Wijelath ES, Murray J, Rahman S, Patel Y, Ishida A, Strand K, Aziz S, Cardona C, Hammond WP, Savidge GF, Rafii S, Sobel M. Novel vascular endothelial growth factor binding domains of fibronectin enhance vascular endothelial growth factor biological activity. Circ. Res. 2002; 91:25–31. [PubMed: 12114318]

Yang JT, Bader BL, Kreidberg JA, Ullman-Cullere M, Trevithick JE, Hynes RO. Overlapping and independent functions of fibronectin receptor integrins in early mesodermal development. Dev. Biol. 1999; 215:264–277. [PubMed: 10545236]

Yang JT, Rayburn H, Hynes RO. Embryonic mesodermal defects in alpha 5 integrin-deficient mice. Development. 1993; 119:1093–1105. [PubMed: 7508365]

Zhang Y, Singh MK, Degenhardt KR, Lu MM, Bennett J, Yoshida Y, Epstein JA. Tie2Cre-mediated inactivation of plexinD1 results in congenital heart, vascular and skeletal defects. Dev. Biol. 2009; 325:82–93. [PubMed: 18992737]

Zhang Z, Huynh T, Baldini A. Mesodermal expression of Tbx1 is necessary and sufficient for pharyngeal arch and cardiac outflow tract development. Development. 2006; 133:3587–3595. [PubMed: 16914493]

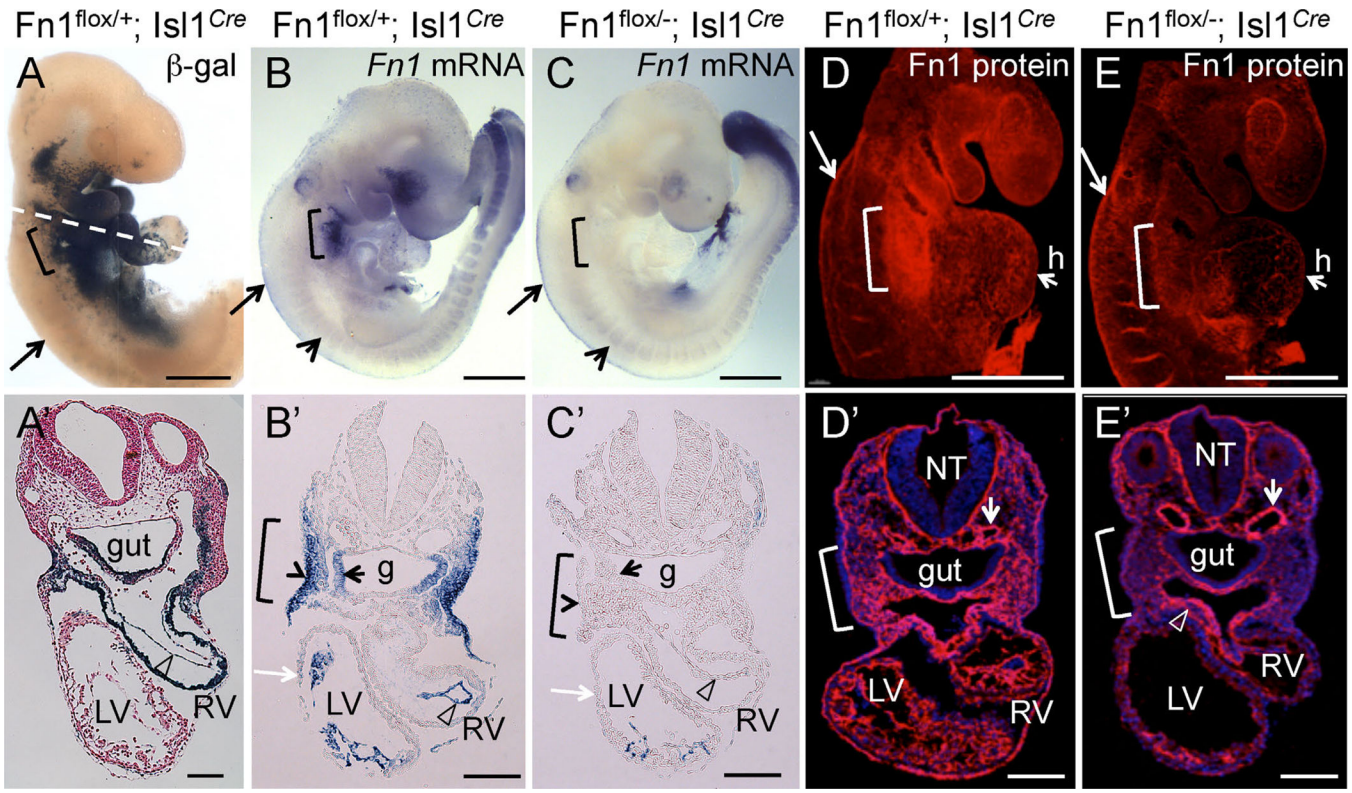

Fig. 1.

Conditional ablation of Fn1 in pharyngeal tissues using the Isl1^{Cre} knock-in strain. All embryos are at E9.5. Brackets in all panels mark the pharyngeal region where arches 3, 4, and 6 will develop. Long arrows in (A–E) point to the neural crest. (A–A′) Fate map of Isl1^{+} cells and their descendants; Dashed line in A marks approximate planes of sections shown in (A′–E′), open arrowhead points to endocardium in A′–C′. (B-B′) *Fn1* mRNA expression is enriched in the surface ectoderm (arrowhead in B′), pharyngeal pocket endoderm (small black arrow), mesoderm, and endocardium (arrowhead). (C-C′). *Fn1* mRNA is ablated in the pharyngeal tissues following Cre-mediated recombination in Fn1$^{flox/-}$; Isl1^{Cre} mutants. Myocardium (white arrow) does not express Fn1. Short arrows in (B–C) point to somites, where Isl1^{Cre} is not expressed and *Fn1* expression is unaltered. (D) Expression of Fn1 protein is enriched in the posterior pharyngeal arches (bracket). E. Fn1 protein is depleted from the pharyngeal region in Fn1$^{flox/-}$; Isl1^{Cre} mutants. (D′–E′) Transverse sections through (D–E). Fn1 is depleted in pharyngeal arches and the heart (h) in Fn1^{flox-}; Isl1^{Cre} mutants (E′). Fn1 remains expressed by the neural crest-derived cells (arrowhead in E′) and by more dorsal regions, including the dorsal aorta (short arrows in D′–E′); g - gut, LV, RV - left and right ventricles, NT - neural tube. Scale bars in (A–E) are 500 μm; in (A′–E′) 100 μm.

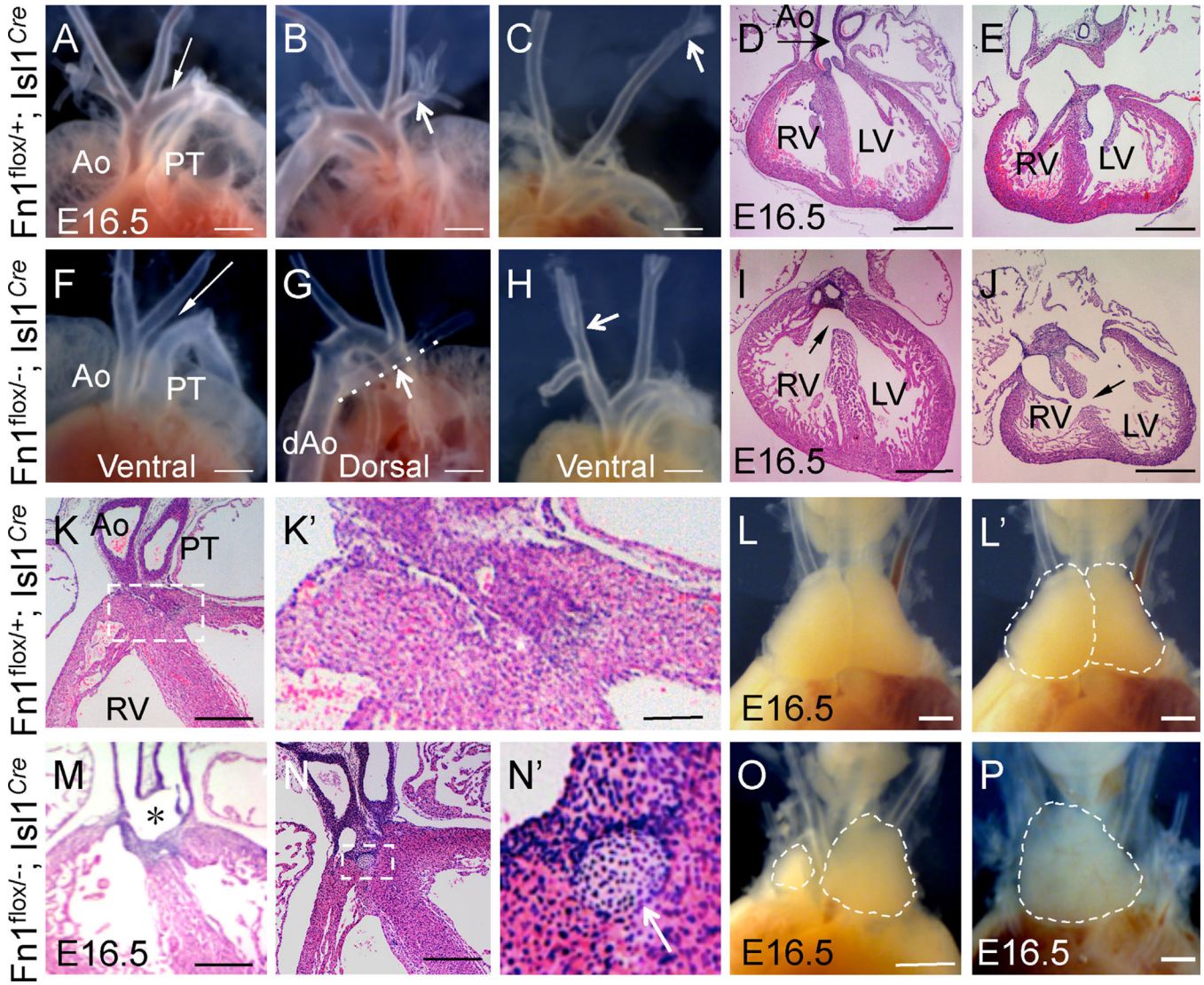

Fig. 2.

Cardiovascular and thymus defects in Fn1$^{flox/-}$; Isl1^{Cre} mutants at E16.5. (A–E) Fn1$^{flox/+}$; Isl1^{Cre} controls. (F–J) Fn1$^{flox/-}$; Isl1^{Cre} mutants. All sections are cut in a coronal orientation and stained with H&E. A. Ventral view. Ao - ascending aorta, PT - pulmonary trunk; arrow points to the arch of aorta. (B) Dorsal view, arrow points to the right subclavian artery. (C) Ventral view, arrow points to a high branch-point of the left carotid artery. (D–E) Complete septum separates the right and left ventricles (RV and LV). Aorta (arrow) originates from the LV. (F) Arrow points to the absent aortic arch. (G) Arrow and the dashed line highlight the right subclavian artery aberrantly originating from the descending aorta, dAo. (H) Arrow points to the low branch point of the right carotid artery. (I) Membranous septum defect, arrow. (J) Muscular septum defect, arrow. H&E stained sections in (D) and (I) and in(E) and (J) show views at equivalent section levels. (K–L′). Fn1$^{flox/+}$; Isl1^{Cre} controls. (M–P) Fn1$^{flox/-}$; Isl1^{Cre} mutants. (K), (K′), (M–N′) are H&E stained sections. (K) Aorta and pulmonary trunk are two separate vessels in controls. K′. Histology of the suboartic region outlined by the dashed box in (K). (L) Thymus. (L′) The same as L, but with the two lobes

outlined by the dashed line. (M) * marks the region where Ao and PT are fused in the $Fn1^{flox/-}$; $Isl1^{Cre}$ mutant. (N–N′) Histology of the subaortic region. The dashed region in (N) is magnified in N′ and shows cartilage-like nodule, white arrow. (O–P) Dashed regions outline the asymmetric thymus lobes in O and a single thymus lobe in (P). Scale bars are 500 μm in all panels, except they are 100 μm in (K), (M), (N) and 10 μm in (K′), (N′).

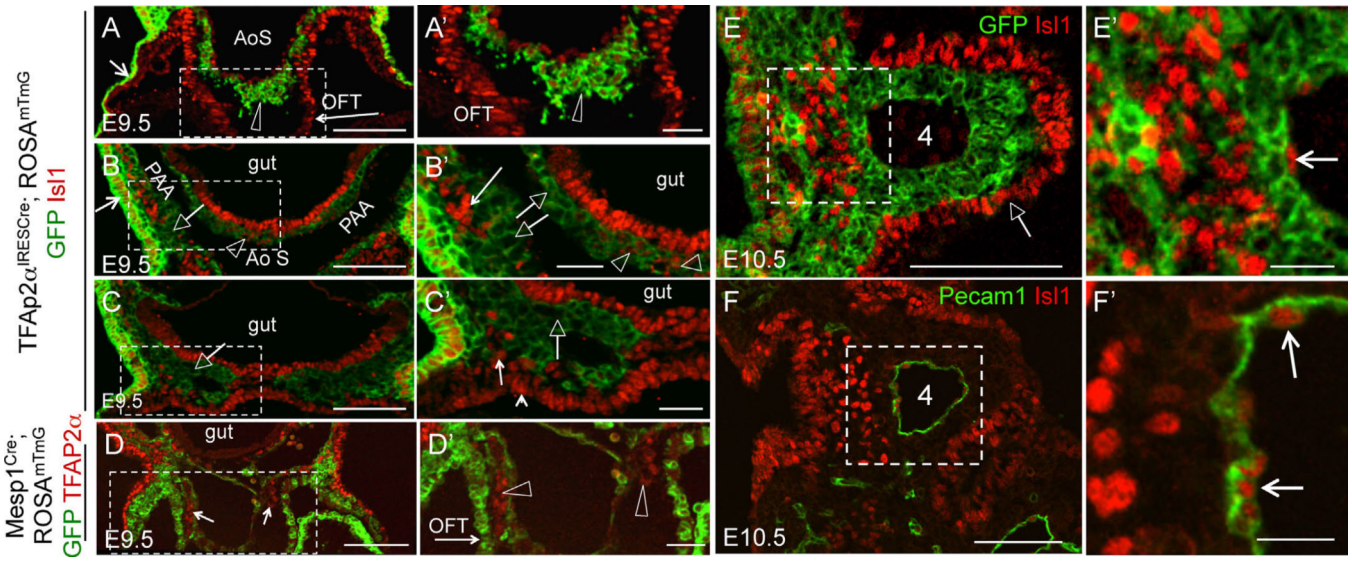

Fig. 3.

Neural crest-derived cells in the cardiac outflow tract express Isl1. (A–C), (A′–C′) Transverse sections through TFAP2α^{IRESCre}; ROSA^{mTmG} embryos isolated at E9.5. Boxed regions in (A–D) are expanded in (A′–D′). (A–C) Fate map of TFAP2α^{IRESCre} - expressing cells and their descendants. GFP (green) marks both the surface ectoderm (short arrows in A–B) and neural crest-derived cells, marked by the open arrowheads and open arrows. Arrowheads point to Isl1^{+} neural crest-derived cells and arrows point to Isl1-negative neural crest cells. Isl1 staining is in red. (A–A′). Section is at the level of the outflow tract (OFT, long arrow). AoS-aortic sac. (B–B′) Section is at the level of the 3rd pharyngeal arch. (C–C′) Section is at the level of the 4th pharyngeal arch. Open arrows point to IslGFP^{+} pharyngeal neural crest cells, arrows in (B′–C′) point to Isl^{+}GFP^{-} pharyngeal mesoderm, and a small arrowhead in (C′) points to Isl^{+}GFP splanchnic mesoderm. (D–D′) E9.5 embryos. Transverse section at the OFT level shows lineage map of Mesp1-derived cells (GFP+, green) and TFAP2α expression (red, small arrows in D). OFT myocardium originates from Mesp1-derived cells (long arrow in D′). TFAP2α^{+}GFP^{-} cells (open arrowheads) in the OFT are not derived from the mesoderm. (E–E′), (F–F′) E10.5 embryos. Boxed areas in (E–F) are expanded in (E′–F′). (E) The majority of neural crest cells in the pharyngeal arches are Isl1GFP^{+}. Isl1^{+}GFP^{-} cells form the arch core mesoderm (boxed in E, expanded in E′) and PAA endothelium (arrows in F′). Native GFP and Tomato fluorescence in all sections were extinguished by mounting sections in 50/50 MeOH/Glycerol, see Methods. Scale bars are 100 μm in (A–D), (E–F), 30 μm in (A′–D′), 20 μm in (E′–F′).

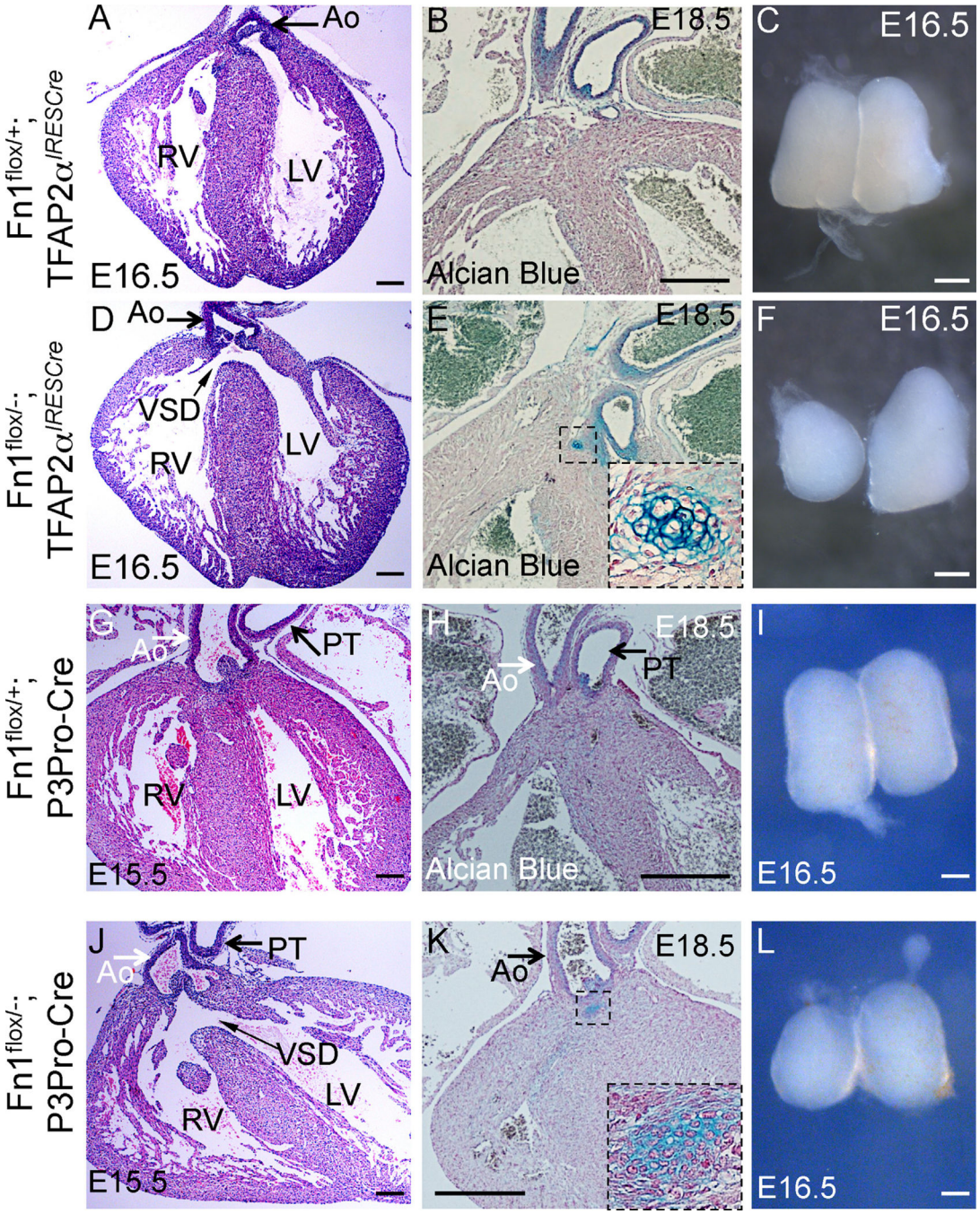

Fig. 4.

Cardiovascular and thymus defects in Fn1$^{flox/-}$; TFAP2α^{IRESCre} mutants at late gestation. (A–C) Fn1$^{flox/+}$; TFAP2α^{IRESCre} controls; (D–F) Fn1$^{flox/-}$; TFAP2α^{IRESCre} mutants; (G–I) Fn1$^{flox/+}$; P3Pro-Cre+ controls; and (J–L) Fn1$^{flox/-}$;P3Pro-Cre+ mutants. All sections were cut in coronal orientation. (A, D, G, J) - H&E staining. Slim arrows in (D) and (J) point to the membranous ventricular septal defect (VSD). Ao - ascending aorta. PT - pulmonary trunk, RV-right ventricle, LV - left ventricle. (B, E, H, K) - Alcian blue and nuclear fast red staining. Cartilage in the mutants is stained in blue (dashed box, expanded in insets of E and

K). (C, F, I, L) - whole isolated thymus lobes. Mutants display hypoplastic and asymmetric thymus lobes (F, L). Scale bars: 100 μm in (A), (D), (G), and (J); 200 μm in (B), (E), (H), and (K); 500 μm in (C), (F), (I), and (L).

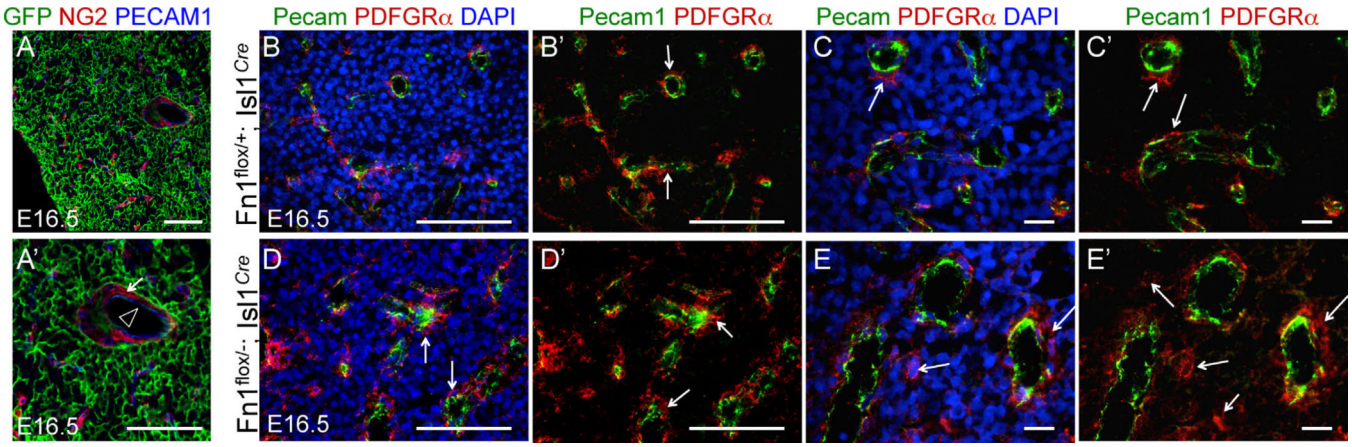

Fig. 5.

Isl1 lineage map of the thymus and thymus vasculature in control and $Fn1^{flox/-}$; $Isl1^{Cre}$ mutants. Sections through the thymus isolated from E16.5 embryos. (A-A′) Section from $Isl1^{Cre}$;$ROSA^{mTmG}$ embryo. The bulk of the thymus and thymus endothelial cells (Pecam1, blue, arrowhead in A′) are derived from $Is1^{+}$ cells. Pericytes (NG2, red, arrows) in the thymus are not of the $Isl1^{+}$ lineage. Thymi from control (B–C) and $Fn1^{flox/-}$; $Isl1^{Cre}$ mutant embryos (D–E) were stained to detect endothelial cells (Pecam1, green), pericytes (PDGFRβ, red, arrows) and nuclei (DAPI, blue). 40 × (B–B′; D–D′) and 63 × (C–C′, E–E′) images are shown. All scale bars are 100 μm, except in C–C′ and E–E′, where they are 10 μm.

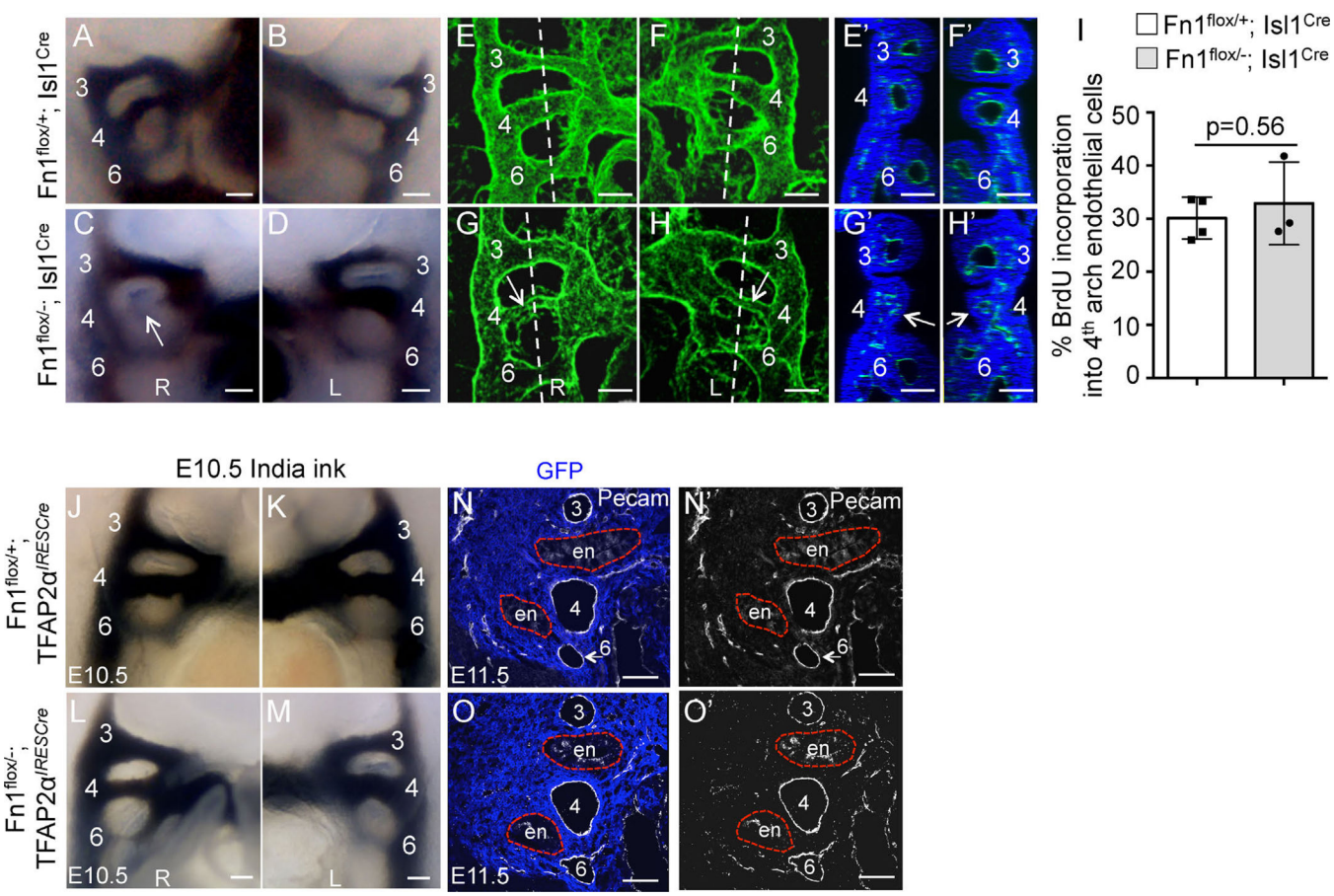

Fig. 6.

Expression of Fn1 in the Isl1-derived tissues regulates formation of the 4th PAAs. All images in (A–M) are from E10.5 embryos. PAAs are numbered. (A–D) Intracardiac India ink injections label the PAAs. All PAAs are visible in controls (A–B). The right 4th PAA (arrow) is non-patent in the $Fn1^{flox/-}$; $Isl1^{Cre}$ mutant (C–D). E-H. Whole mount Pecam1 staining (green) and 3D–confocal image reconstruction show well-formed PAAs in controls (E–F), and bi-laterally thin 4th PAAs in the $Fn1^{flox/-}$; $Isl1^{Cre}$ mutant, arrows (G–H). Dashed lines in (E–H) mark optical planes of section shown in (E′–H′). Pecam1 (blood vessels, green) and DRAQ5 (nuclei, blue). Arrows point to pharyngeal arches with thin/disorganized PAAs. Scale bars are 100 μm; R - right, L - left. I. BrdU incorporation into endothelial cells in controls (white bars) and mutant (gray bars) embryos; Each dot represents measurements in one pharyngeal arch; p was determined using 2-tailed, unpaired Student′s *t* test. (J–O′) Expression of Fn1 in the neural crest and the surface ectoderm is not required for PAA formation. (J–M) India ink injections at E10.5. All PAAs are visible in control $Fn1^{flox/+}$; $TFAP2\alpha^{IRESCre}$ and mutant $Fn1^{flox/-}$; $TFAP2\alpha^{IRESCre}$ embryos at E10.5. (N–O′) Coronal sections through E11.5 embryos show that all PAAs (numbered 3–6) are formed normally in control $Fn1^{flox/+}$; $TFAP2\alpha^{IRESCre}$ and mutant $Fn1^{flox/-}$; $TFAP2\alpha^{IRESCre}$ embryos. Neural crest is stained using anti-GFP antibodies (blue), due to the presence of the $ROSA^{mTmG}$ allele and endothelium is labeled with anti-Pecam1 antibodies (white). Red dashed lines

outline the endoderm (en). Native GFP and tdTomato fluorescence was extinguished by boiling sections in 10 mM Citric Acid pH 6.0 as described in Methods.

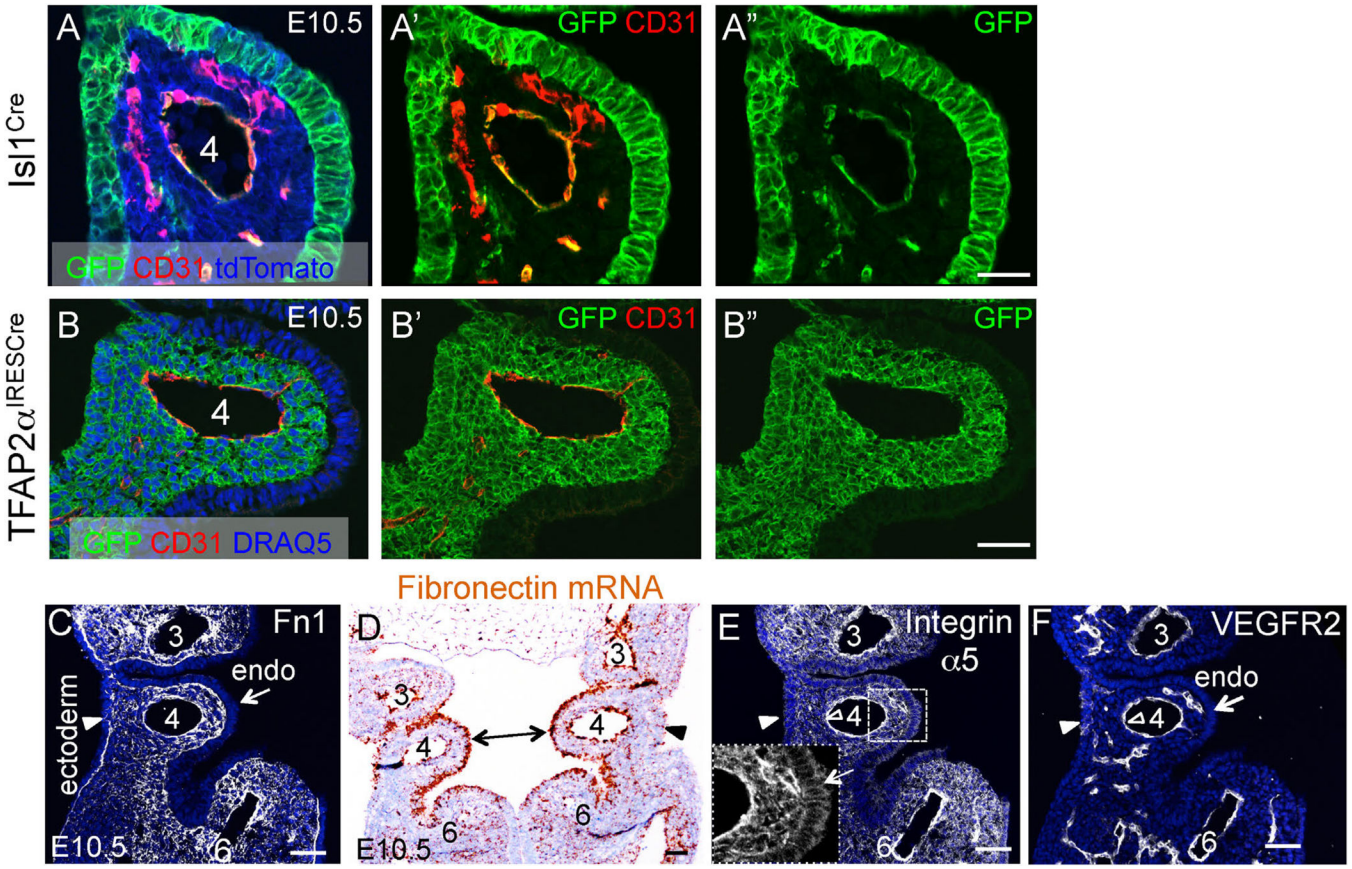

Fig. 7.

Lineages labeled in the Isl1^{Cre} and TFAP2α^{IRESCre} strains and expression patterns of Fn1 and integrin α5 in the 4th pharyngeal arch at E10.5. (A–A″) Isl1^{Cre}; ROSA^{mTmG}. (B–B″) TFAP2α^{IRESCre}; ROSA^{mTmG}. Native GFP and tdTomato fluorescence was extinguished by boiling in 10 mM Citric Acid pH 6.0 as described in Methods. C. Fn1 protein (white). (D) *Fn1* mRNA (brown). (E) Integrin α5 protein (white); Arrows in the inset point to integrin α5 expression in the endoderm. (F) Same section as in (E) co-stained with antibodies to VEGFR2 (white). Endo–endoderm; arrowheads point to ectoderm; Pharyngeal arches are numbered; Scale bars in (A–B) 30 μm; scale bars in (C–F) 50 μm.

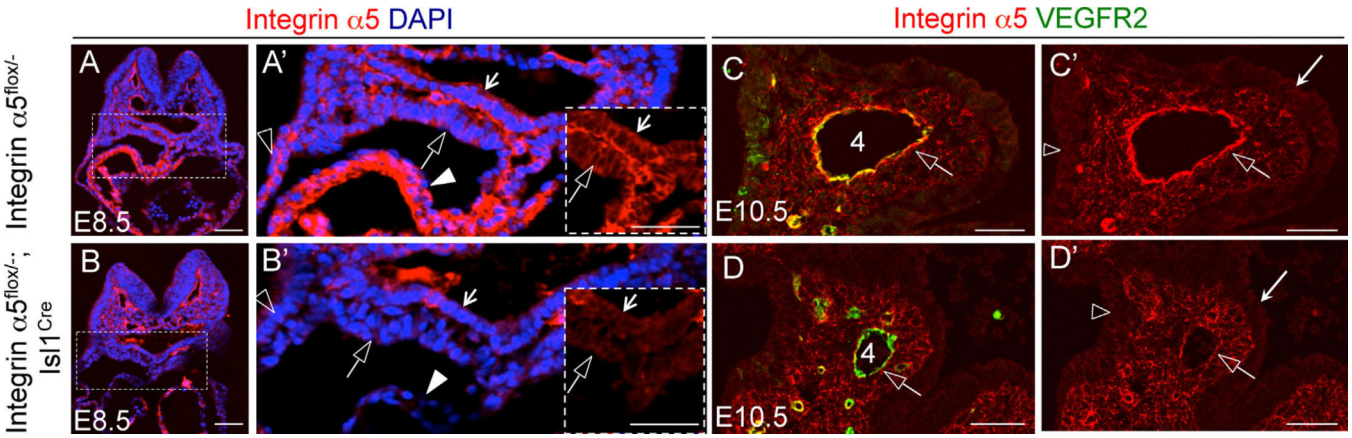

Fig. 8.

Ablation of integrin α5 using the Isl1*Cre* strain. (A–B) Transverse sections through E8.5 embryos. Integrin α5 – red, nuclei – blue. (A–A′) Control. (B–B′) Mutant. Boxed regions in A and B are expanded in A′ and B′. Arrows – endoderm; open arrows – splanchnic mesoderm; closed arrowheads – myocardium; open arrowheads – ectoderm. (C–D) Coronal sections through the 4th pharyngeal arch in E10.5 control (C, C′) and mutant (D, D′) embryos. Integrin α5 – red, VEGFR2 (endothelium) – green. Open arrows point to PAA endothelium; Long arrows in (C′), (D′) point to the endoderm;. All scale bars are 50 μm.

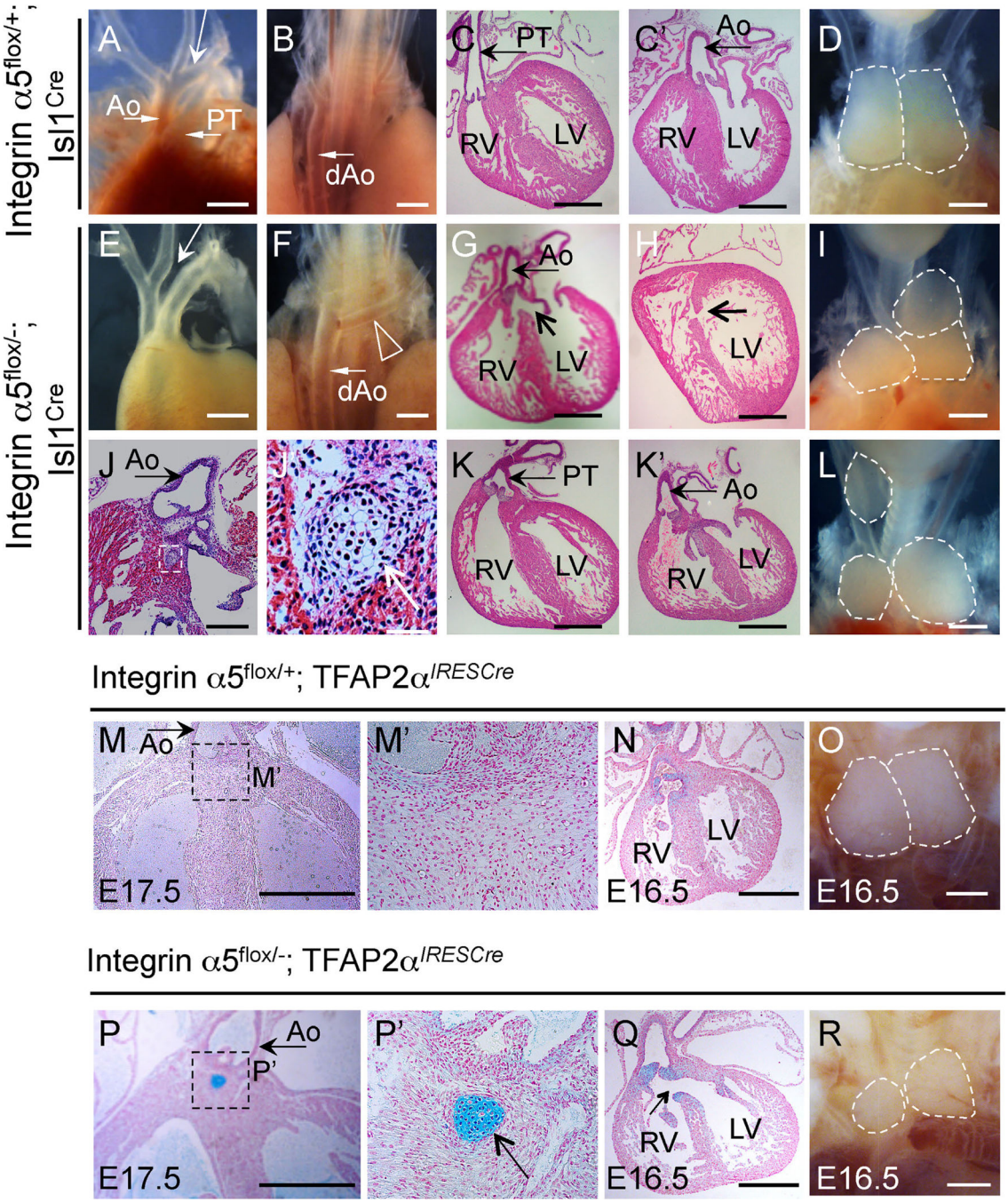

Fig. 9.

Cardiovascular and thymus defects inintegrin $\alpha5^{flox/-}$; $Isl1^{Cre}$and in integrin $\alpha5^{flox/-}$; $TFAP2\alpha^{IRESCre}$ mutants at E16.5 and E17.5. (A–D) Controls; E-L Mutants. (A, E, D, I, L) - ventral views; (B, F) - dorsal views. Ao - ascending aorta; PT - pulmonary trunk; Long arrow in A points to the aortic arch; dAo-descending aorta is marked in (B). (C) PT originates from the right ventricle (RV) in controls; Ao originates from the left ventricle (LV) in controls; (D) two symmetrical thymus lobes of a control embryo are outlined. (E) Arrow points to the missing aortic arch; (F) Arrowhead points to the subclavian artery

originating from the dAo. (G) Arrow points to the membranous ventricular septal defect (VSD); This mutant also has an overriding aorta, receiving the blood from the RV and LV. (H) Arrow points to the muscular septal defect in the mutant. (I, L). Three thymus lobes are outlined in the mutants. (J–J′) Subaortic cartilage nodule in the mutant (boxed). The box in J is expanded in (J′), arrow in (J′) points to the cartilage. (K–K′) Double outlet right ventricle: both the PT (K) and Ao (K′) originate from the right ventricle in this mutant. (M–O). Integrin $\alpha 5^{flox/+}$; TFAP2α^{IRESCre} controls. (P–R) Integrin $\alpha 5^{flox/-}$; TFAP2α^{IRESCre} mutants. All sections were cut in coronal orientation and stained with Alcian blue and nuclear fast red. Boxed regions in M and (P) are expanded in (M ‘) and (P′). Cartilage in the mutants is stained blue (boxed region in P and arrow in P′). Arrow in (Q) points to the membranous VSD. Asymmetric and hypoplastic thymus lobes in integrin $\alpha 5^{flox/-}$; TFAP2α^{IRESCre} mutant are outlined in (R). All scale bars are 500 μm, except they are 100 μm in (J) and 50 μm in (J′).

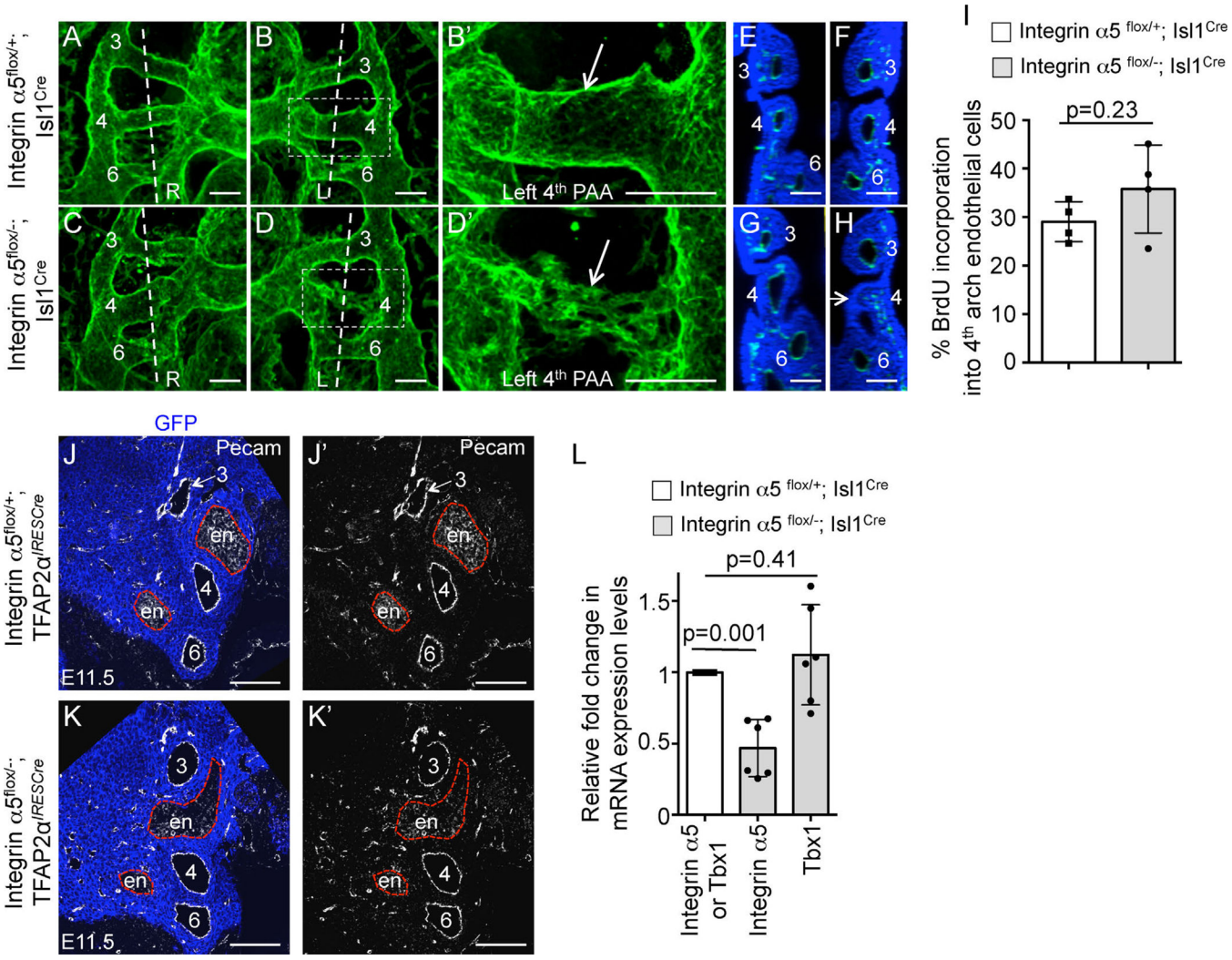

Fig. 10.

PAA defects in $\alpha5^{flox/-}$; $Isl1^{Cre}$ mutants at E10.5. (A–D) 3D reconstructions of whole mount confocal data from Pecam1-stained embryos. L-left; R-right. Each PAA is labeled. The boxed regions in (B) and (D) are expanded in (B′) and (D′). Arrows point to the 4th PAAs in the control and mutant. Vertical doted lines are the planes of sections shown in (E–F) and (G–H). (E, G) - right sides; (F, H) - left sides. Arrow in (H) points to the 4th arch with the defective PAA. All scale bars are 100 μm. (I) BrdU incorporation into endothelial cells in the 4th pharyngeal arches. (J-J′), (K-K′). Coronal sections through E11.5 pharyngeal regions in integrin $\alpha5^{flox/+}$; $TFAP2\alpha^{IRESCre}$ control (J-J′) and integrin $\alpha5^{flox/-}$; $TFAP2\alpha^{IRESCre}$ mutant (K-K′) embryos. PAAs (numbered 3–6) form normally in control $Fn1^{flox/+}$;$TFAP2\alpha^{IRESCre}$ and mutant $Fn1^{flox/-}$; $TFAP2\alpha^{IRESCre}$ embryos. Neural crest is stained using anti-GFP antibodies (blue), due to the presence of the $ROSA^{mTmG}$ allele and the endothelium is labeled with anti-Pecam1 antibodies (white). Red dashed lines outline the endoderm (en). Native GFP and tdTomato fluorescence was extinguished by boiling in 10 mM Citric Acid, pH 6.0 as described in Methods. (L) Expression levels of *integrin α5* and *Tbx1* mRNA in the mutants (gray bars) were normalized to those of control embryos (white

bar). For (I) and (L): each data point represents one arch; p was determined using 2-tailed, unpaired Student's t test.

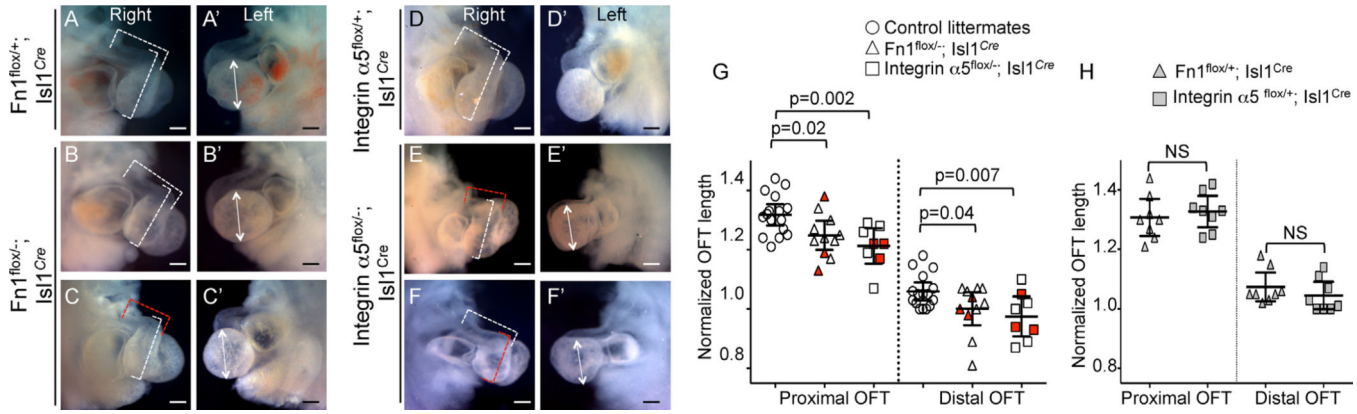

Fig. 11.

Defects in OFT elongation in Fn1$^{flox/-}$; Isl1^{Cre} and integrin α5$^{flox/-}$; Isl1^{Cre} mutants are not correlated with the defects in PAA formation at E10.5. In A-F. Dotted brackets mark the lengths of the distal and proximal OFT. Red brackets mark OFT lengths that differ from controls, white brackets mark OFT lengths that are similar to controls. (A′-F′) Double-headed arrows mark the heights of the left ventricle. (A-C, D-F) Right side views. (A′-C′, D′-F′) Left side views. All scale bars are 200 μm. G. Normalized lengths of the proximal and distal OFT. Red symbols mark embryos with defective PAAs. Control embryos, (unfilled circles) were collected from Fn1 and integrin α5 crosses and their genotypes are marked in H. H. Normalized OFT lengths in control embryos from Fn1 and integrin α5 crosses. (G–H) Each symbol represents one embryo. *p*-Value was determined using 2-tailed, unpaired Student's *t* test.

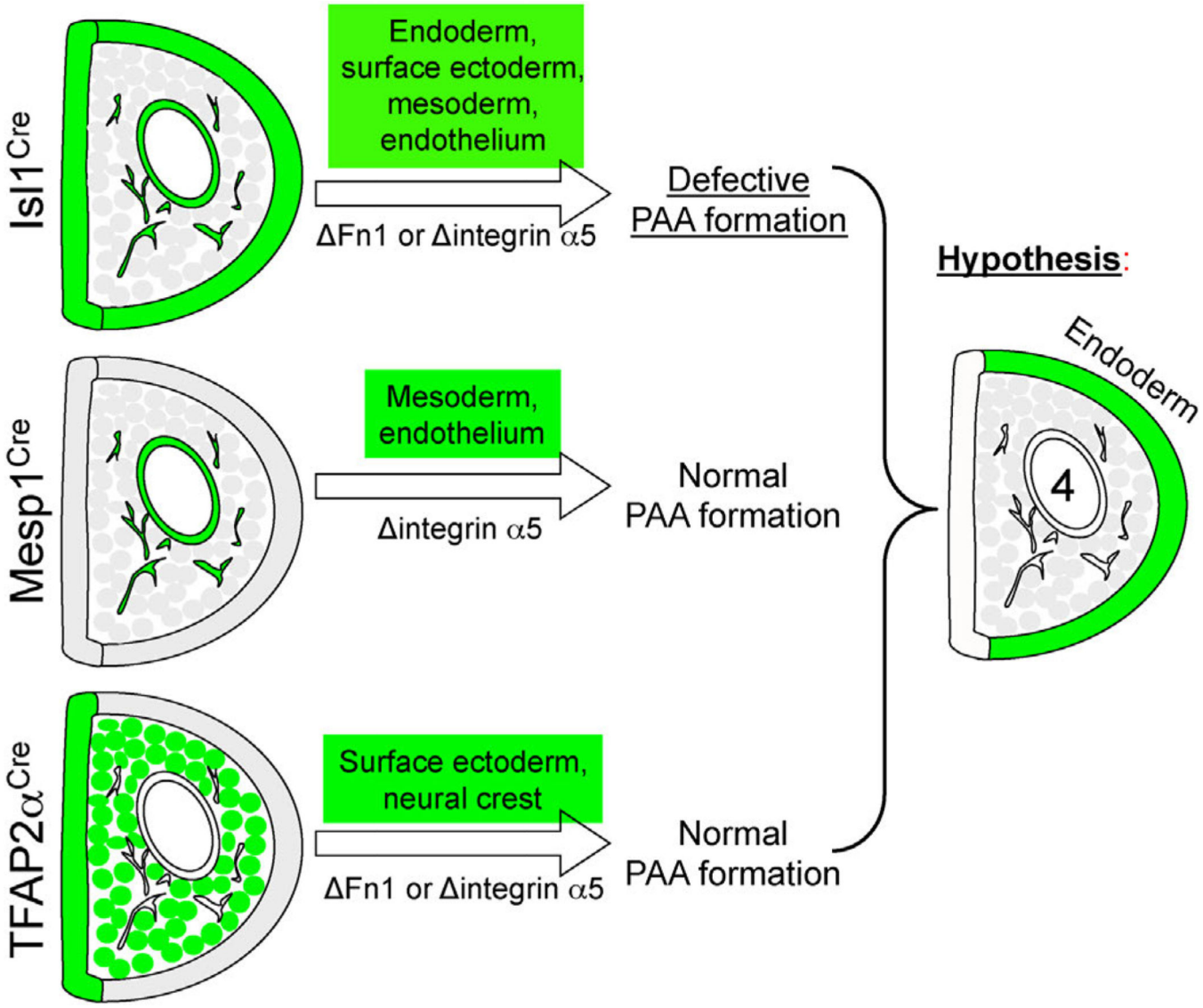

Fig. 12.

Summary of PAA formation phenotypes resulting from the ablation of integrin α5 using the Isl1^{Cre}, Mesp1^{Cre}, and TFAP2α^{IRESCre} strains. Green color marks the tissues in which integrin α5 was ablated in each strain. We hypothesize that an integrin α5-dependent signal in the pharyngeal endoderm regulates PAA formation.

Table 1

Conditional knockout of Fn1 using the Isl1^{Cre} strain is embryonic and neonatal lethal.

Age	Total # of embryos	Fn1$^{flox/+}$	Fn1$^{flox/+}$; Isl1^{Cre}	Fn1$^{flox/-}$	Fn1$^{flox/-}$; Isl1^{Cre}
E8.5–9.5	386	88(23%)	88(23%)	101(26%)	109(28%)
E10.5	342	88(26%)	87(25%)	83(24%)	84(25%)
E13.5–18.5	179	46(26%)	58(32%)	51(28%)	24(13%)
3 weeks	188	66(35%)	49(34%)	50(29%)	9(5%)

Each column reports the number of embryos or mice (at 3 weeks) observed of each genotype

Dev Biol. Author manuscript; available in PMC 2017 February 16.

Table 2

Cardiovascular and thymus defects in individual $Fn1^{flox/-}$; $Isl1^{Cre}$ mutants.

Embryo #	Stage	3rd PAA-related	4th PAA-related	Alignment of the great vessels	Membranous VSD and sub-aortic cartilage	Muscular VSD, myocardial defects	Thymus
1	E15.5	N/E	N/A	N/A	Membranous VSD, peri-aortic nodule	N/A	Slightly asymmetric
2	E15.5	ABCCA	RERSA	N/A	peri-aortic nodule	N/A	R hypoplastic (moderate)
3	E16.5	N/E	N/A	N/A	Membranous VSD	N/A	Slightly asymmetric
4	E16.5	N/E	RERSA	N/A	N/A	Muscular VSD	Slightly asymmetric
5	E16.5	N/E	IAA-B	N/A	Membranous VSD, PTA (Van Praagh A4)	N/A	R/L ectopic; L fragmented
6	E16.5	ABCCA	N/A	N/A	Peri-aortic nodule	N/A	Slightly asymmetric
7	E16.5	ABCCA	N/A	N/A	Peri-aortic nodule	N/A	L hypoplastic (moderate)
8	E17.5	ABCCA	N/A	N/A	Peri-aortic nodule	Muscular VSD	Single fused lobe
9	E17.5	ABCCA	N/A	N/A	N/A	N/A	R hypoplastic (severe)
10	E17.5	N/A	RERSA	N/A	Peri-aortic nodule	Reduced compact zone (RV)/trabeculation (RV+LV)	L fragmented
11	E18.5	N/A	N/A	N/A	Peri-aortic nodule	Muscular VSD	R hypoplastic (severe)
12	E18.5	N/E	IAA-B	DORV	N/E	N/E	N/E
Summary		**5/7 (71%)**	**5/12 (42%)**	**1/12 (8%)**	**9/11 (82%)**	**4/11 (36%)**	**7/11 (64%)**

Abbreviations: AAA – aortic arch artery; ABCCA – aberrant branch point of common carotid artery; DA – ductus arteriosus; DORV – double outlet right ventricle; IAA-B – interrupted aortic arch type B; L – left, R – right; N/A – not affected; N/E – not examined; OA – overriding aorta; PTA – persistent truncus arteriosus; RERSA – retroesophageal right subclavian artery; VSD – ventricular septal defect.

Table 3

PAA formation in $Fn1^{flox/-}$; $Isl1^{Cre}$ mutants.

Embryo number	Number of somites	Method of analysis	Right 4th PAA	Left 4th PAA
1	36–40	PECAM1/confocal	Thin	Thin
2	36–40	PECAM1/confocal	Thin	4th PA absent
3	36–40	PECAM1/confocal	Grossly normal	Thin
4	36	PECAM1/confocal	Grossly normal	Grossly normal
5	36	PECAM1/confocal	Grossly normal	Grossly normal
6	37	PECAM1/confocal	Grossly normal	Grossly normal
7	36–40	PECAM1/confocal	Grossly normal	Grossly normal
8	36–40	PECAM1/confocal	Grossly normal	Grossly normal
9	36–40	PECAM1/confocal	Grossly normal	Grossly normal
10	36–40	PECAM1/confocal	Grossly normal	Grossly normal
11	3 6 –40	PECAM1/confocal	Grossly normal	Grossly normal
12	36–40	PECAM1/confocal	Grossly normal	Grossly normal
13	36	Intracardiac ink injection	Thin	Grossly normal
14	37	Intracardiac ink injection	Thin	Grossly normal
15	36–40	Intracardiac ink injection	Thin	Grossly normal
16	36–40	Intracardiac ink injection	Thin	Grossly normal
17	3 6 –40	Intracardiac ink injection	Thin	Grossly normal

Penetrance: 8/18=44%(embryos); 9/35=26% (pharyngeal arches)

Table 4

Conditional knockout of integrin α5 using the Isl1^{Cre} strain is embryonic and neonatal lethal.

Age	Total # of embryos	Integrin α5$^{flox/+}$	Integrin α5$^{flox/+}$; Isl1^{Cre}	integrin α5$^{flox/-}$	Integrin α5$^{flox/-}$; Isl1^{Cre}
E8.5–9.5	44	9(20%)	12(27%)	12(27%)	11(25%)
E10.5	169	58(34%)	39(23%)	41(24%)	31(18%)
E13.5–18.5	117	28(24%)	38(32%)	30(26%)	21(18%)
3 weeks	172	61(35%)	49(28%)	61(35%)	1(1%)

Each column reports the number of embryos or mice (at 3 weeks) observed of each genotype

Table 5

Cardiovascular and thymus defects individual integrin α5 $^{flox/-}$; Isl1^{Cre} mutants.

Embryo #	Stage	3rd PAA-related	4th PAA-related	Alignment of the great vessels	Membranous VSD and sub-aortic cartilage	Muscular VSD, myocardial defects	Thymus
1	E17.5	N/A	N/A	DORV, PT atresia, DA absent	Membranous VSD	N/A	Slightly asymmetric
2	E17.5	ABCCA	IAA-B	DORV	Membranous VSD	N/A	Slightly asymmetric
3	E17.5	N/A	RERSA	N/A	Membranous VSD	N/A	R hypoplastic (moderate)
4	E17.5	N/A	N/A	N/A	Membranous VSD, peri-aortic nodule	Muscular VSD, RV+LV reduced trabeculation	L hypoplastic (moderate)
5	E17.5	N/A	N/A	DORV	N/E	N/E	Slightly asymmetric
6	E17.5	N/A	RERSA	N/A	N/E	N/E	R hypoplastic (severe)
7	e16.5	N/A	IAA-B	OA	Membranous VSD	Muscular VSD	Slightly asymmetric
8	e16.5	ABCCA	IAA-B	N/A	N/A	Muscular VSD	R hypoplastic (severe); additional ectopic R lobe
9	e16.5	N/A	N/A	N/A	Peri-aortic nodule	N/A	R hypoplastic (severe)
10	e18.5	N/A	N/A	N/A	Membranous VSD, peri-aortic nodule	N/A	L hypoplastic (severe), additional ectopic L lobe
Summary		**2/10 (20%)**	**5/10 (50%)**	**4/10 (40%)**	**7/8 (88%)**	**3/8 (38%)**	**6/10 (60%)**

Abbreviations: AAA – aortic arch artery; ABCCA – aberrant branch point of common carotid artery; DA – ductus arteriosus; DORV – double outlet right ventricle; IAA-B – interrupted aortic arch type B; L – left, R – right; N/A – not affected; N/E – not examined; OA – overriding aorta; PT – pulmonary trunk; RERSA – retroesophageal right subclavian artery; VSD – ventricular septal defect.

Table 6

PAA formation in individual integrin α5 $^{flox/-}$; Isl1^{Cre} mutants.

Embryo number	Number of somites	Method of analysis	Right 4th PAA	Left 4th PAA
1	37	PECAM1/confocal	Thin	Thin
2	36	PECAM1/confocal	Thin	Grossly normal
3	36	PECAM1/confocal	Thin	Thin (mild)
4	36–40	PECAM1/confocal	Grossly normal	All plexus (no main artery)
5	36–40	PECAM1/confocal	Grossly normal	Thin
6	36–40	PECAM1/confocal	Thin	Grossly normal
7	36–40	PECAM1/confocal	Grossly normal	Grossly normal
8	36–40	PECAM1/confocal	Grossly normal	Grossly normal
9	36–40	PECAM1/confocal	Grossly normal	Grossly normal
10	36–40	PECAM1/confocal	Grossly normal	Grossly normal
11	36 –40	PECAM1/confocal	Grossly normal	Grossly normal
12	36–40	Intracardiac ink injection	Thin	Grossly normal
13	36–40	Intracardiac ink injection	Thin	Not patent in the middle
14	36–40	Intracardiac ink injection	Not patent	Grossly normal
15	36–40	Intracardiac ink injection	Not patent	Thin
16	36–40	Intracardiac ink injection	Not patent	Thin
17	36–40	Intracardiac ink injection	Grossly normal	Grossly normal
18	36–40	Intracardiac ink injection	Grossly normal	Grossly normal

Penetrance: 11/18 = 61% (embryos); 16/36 = 44% (pharyngeal arches)